**Luís Gabriel Curado
dos Santos**

**Estabelecimento de uma metodologia de análise
integrada da interação pneu-pavimento**

Establishment of an integrated analysis methodology of
tire-pavement interaction

**Luís Gabriel Curado
dos Santos**

**Estabelecimento de uma metodologia de análise
integrada da interação pneu-pavimento**

Establishment of an integrated analysis methodology of
tire-pavement interaction

o júri / the jury

presidente / president   **Prof. Doutora Margarida Isabel Cabrita Marques Coelho**
Prof. Auxiliar da Universidade de Aveiro

Prof. Doutor Marco Paulo Lages Parente
Professor auxiliar da *Faculdade de Engenharia da Universidade de Porto*

Prof. Doutor Robertt Valente
Professor associado do departamento de Engenharia Mecânica da Universidade de Aveiro (orientador)

agradecimentos /
acknowledgements

abstract

Approximately 4940 thousand tonnes of tires are produced annually in Europe. Some of the particles emitted by tire wear can have a negative impact on the environment. In addition, tires are negatively influenced by driving dynamics, and the risk of aquaplaning can have fatal consequences. The main objective of the present work is the study of an integrated analysis of the tire-pavement interaction phenomenon, based on the evaluation of the tire wear during rolling, the changes in the friction coefficient and the tire inflation pressure.

First, a bibliographic search was performed to gather information about the physics behind the motion of a tire, representative models of a tire and, finally, the Archard wear model for simulating the tire tread wear.

In the second part of the dissertation, an axyssimetric model of the tire was built in order to perform the Finite Element Analysis (FEA), using Abaqus software.

In the third part, pressurization of the tire model was carried out and then an imposed displacement step was induced in order to compress the tire tread against the surface. After the compressing step, a mathematical model based on the Archard wear model was initiated as a sub-routine for the calculation (and for prior visualization) of the wear occurred in the tire. The obtained wear depth, after each run of a varying inflation pressure and friction coefficient, provided a clear demonstration of the direct relationship between the friction coefficient and the ablation rate of a surface. Furthermore, mathematical equations were built for each friction coefficients in order to predict wear for different friction coefficients, and for different inflation pressures.

resumo

Cerca de 4940 mil toneladas de pneus são produzidos anualmente na Europa. Algumas das partículas emitidas pelo desgaste dos pneus podem ter um impacto negativo sobre o meio ambiente. Além disso, os pneus são negativamente influenciados pela dinâmica de condução, e o risco de aquaplanagem pode ter consequências fatais.

O objetivo principal do trabalho apresentado é o estudo de um sistema de análise integrada do fenómeno de interação pneu-pavimento, baseado na avaliação do desgaste dos pneus durante o rolamento, alterando o coeficiente de atrito do pavimento e a pressão dos pneus. Primeiro, foi realizada uma busca bibliográfica com o intuito de obter informações sobre a física por de trás do movimento de um pneu, modelos representativos de um pneu e, finalmente, do modelo de desgaste de Archard para simular o desgaste do piso do pneu.

Na segunda parte da dissertação, um modelo axissimétrico do pneu foi construído para realizar a Análise de Elementos Finitos (AEF) usando o software Abaqus.

Na terceira parte, foi realizada a pressurização do modelo de pneu e, em seguida, foi induzido o deslocamento de uma carga a fim de comprimir o piso do pneu contra o pavimento. Após a etapa de compressão, um modelo matemático baseado no modelo de desgaste de Archard foi iniciado como uma sub-rotina para o cálculo e visualização prévia do desgaste ocorrido no pneu.

A profundidade de desgaste obtida, após cada execução de uma pressão de insuflação variável e um coeficiente de atrito variável, forneceu uma demonstração clara da relação direta entre o coeficiente de atrito e a taxa de ablação de uma superfície. Além disso, foram desenvolvidas equações matemáticas para cada coeficiente de atrito, a fim de prever o desgaste dentro de cada coeficiente de atrito para cada pressão de insuflação diferente.

Contents

Intentionally blank page.

List of Tables

Intentionally blank page.

List of Figures

Part I

Introduction and Background

Chapter 1

Introduction

1.1 Motivation

Pneumatic tires play an important role in the human being's life, since the main source of transportation moves on pneumatic tires, which provides a smooth ride. This status was achieved after more than one hundred years' of tire evolution, since the initial invention of the pneumatic tire by John Boyd Dunlop around 1890 [1].

With the growing demand for pneumatic tires, many improvements have been made since the early models, such as reinforcement cords, bead, vulcanization process, different materials and the introduction of the tubeless tire, among others developments. A tire has multiple functions, not only supporting the weight and cushion the irregularities of the pavement, but also providing the desired braking/traction and lateral force for the vehicle control. Furthermore, concerns regarding the environment are an extra requirement for the development of tire technologies. These concerns include the waste of energy due to rolling resistance, the pollution through the emission of tire compounds, etc.

In order to keep up with the innovation, engineering is shifting their resources to a cheaper and faster approach towards tire development, such as the Finite Element Method (FEM). The use of software to predict performance outcomes, such as the rolling resistance, grip, noise, vibration and harshness (NVH), contributes to save every day thousands of Euros and hours in development. Additionally, modelling and numerical simulation in early development stages allows field testing to be made on a later stage, which means less money spent in manufacturing tire prototypes. In addition, these software tools allow the management and assessment of a multitude of factors that are otherwise impossible to be taken into account. It is important to make prediction software faster and reliable, adapting it to specific problems and balancing the simplifications with the accuracy of results. It is also important to understand the connection between mechanical properties, performance parameters, safety parameters and, last, but not least, pollution.

1.2   Main goals and methodology

The work goal of this dissertation is to establish a correlation between tire inflation and tire-road friction in order to set the road performance parameters regarding the tire ablation. To do so, a Finite Element software called Abaqus was used as the main framework for this study.

Several tire modelling techniques have been developed by researchers with the main purpose of computational time reduction, such as axyssimetric tire modelling [2, 3]. The present dissertation has roots in the work study by S. Palanivelu *et al.* [2], therefore, an axyssimetric approach to tire modelling was carried out based on a 205/55R16 tire with the aim of generate the 3-D model, the Yeoh hyperelastic model was used to characterize tire reinforcements and rubber/tread.

The Finite Element analysis begins with the inflation of the 205/55 R16 tire to the described pressure (220, 240, 250, 280 and 300 kPa), and then, the contact between the tire and the road surface. The contact is between two surfaces, the outer surface of the tire (tread) and an analytical rigid surface. The definition of the contact trough the surface interaction is by means of a penalty friction formula, for a tangential behavior, and a Lagrange constraint enforcement method, for the normal behavior.

Then a steady-state rolling analysis was conducted with a penalty friction coefficient values of 0.8, 1.0, 1.1, 1.3 alongside with an Abaqus subroutine to simulate the wear under a cycle of 50000 seconds, which corresponds to a 555,5 km run.

The change in the tire inflation pressure is intented for a better understanding on how the tire would react for different type of users, since not everyone respects the tire pressure usage. The friction coefficient is set to the different values above, for a better understating on how changing the friction coefficient could affect the tire ablation. Finally, with the analysis of the changing of the ablation with pressurization and friction coefficient, a correlation is developed in order to predict the wear under different pressures for equal cycles and friction coefficients.

1.3   Reading guide

This Dissertation is divided into six chapters.The Chapter 1, Introduction, presents and synthesizes the motivation, the goals and the methodologies to be followed.

In Chapter 2, referred to as the "State of the Art", a brief overview of the important subjects addressed in this dissertation is presented and supported by literature results. This literature survey also aims to help the understanding of the goals set.

Chapter 3 intends to present and describe the tire structures, as well as the Abaqus modelling process, from the axyssimetric section to the 3D model of the tire.

In Chapter 4, analysis of the tires footprint for different pressurization pressures are provided, together with the steady state rolling of the tire, as well as the process of implementing the Archard wear model as an Abaqus subroutine.

Chapter 5, Results and Discussion, aims to analyze and discuss on the obtained results.

Chapter 6, Conclusion, presents the most important outcomes of the dissertation, highlighting the main ideas obtained with this research work.

Chapter 2

State of the art review

Tires function as an interface between vehicles and the pavement. The tire is an air-filled structure, which provides a cushion to support the vehicle weight and to filter road irregularities for a smooth ride. Additionally, all forces and moments needed for driving, braking and cornering are transferred between the vehicle and the road through the outside tire surface. The force generation capacity of the tire is a function of the tire-road contact properties and tire deflection, which in turn is influenced by the overall tire structural design and material properties.

2.1   Steps in the development of the pneumatic tyre

For more than 5,000 years, the wheel has been reinvented at different times and in different regions to meet current transportation needs.

In its earliest forms, the wheel was made as a solid disc with three segments held together by circular pieces of metal or leather. The principle of a disc revolving on an axis was known from pottery, and making the wheel was thus an early example of technology transfer. Later, wooden spoked wheels, but only for superior vehicles like war chariots. Spoked wheels were lighter, stronger and more stable [4].

Spoked wooden wheels lasted until the modern era of coaches, and then usually with iron tyres. Even the first Benz motor car introduced in 1886, which was basically a motorised carriage, still had spoked wooden wheels.

The pneumatic tyre was invented later, firstly for bicycles (Dunlop 1888 [5, 4]) and subsequently for automobiles. In 1898, Continental started producing the so called "pneumatics", tyres capable of giving a more cushioned ride and enabling automobiles to travel at higher speeds. Continental also made a significant contribution towards further technical advances of the pneumatic tyre. From 1904 onwards, tyres featured a tread pattern and were given their typical black colour. The addition of carbon colored tyres in black and made them tougher and more durable [5].

Around 1920 the cord tyre came from the U.S.A[6], a tyre with a body made of cotton cord which was more resilient, less susceptible to punctures, and last for a longer time. The low-pressure tyre or "balloon", inflated under 3 bar was invented around 1920. It was followed in the 1940s by the "super balloon" tyre which had a larger volume of air

and better comfort.

In the early 1950s, the steel radial tyre set new standards in mileage and handling performance, and by 1970 low profile tyres were invented [7, 5].

Modern passenger car radials are composed of up to 25 different structural parts and as many as 12 different rubber compounds. The main structural elements are the casing and the tread/belt assembly. The casing cushions the tyre and contains the required volume of air, as it is the load carrier. The tread/belt assembly envelopes the casing and provides for low rolling resistance, optimum driving behaviour and mileage. The tread/belt assembly provides a minimal rolling resistance and a better handling [7].

2.2   Tire forces and moments

In order to analyze the forces and moments which are acting on a tire surface, especially during cornering, we need to define a coordinate system. Since the wheel can move in three directions, we need a 3-D coordinate system. There are several axis systems defined, the most common being the tire axis system, defined by the Society of Automotive Engineers (SAE) and by ISO, the International Organization for Standardization, as shown in Figure 2 [8, 7].
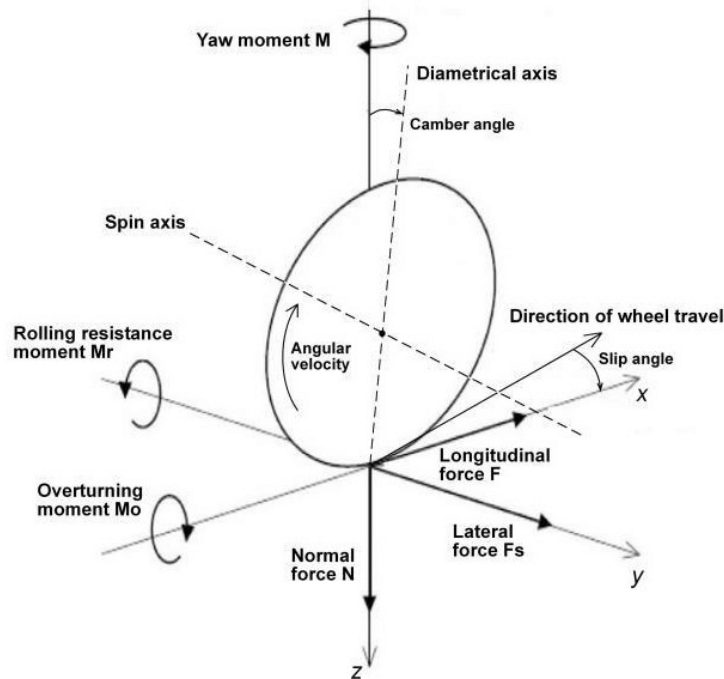
Figure 2.1: Tire coordinate system by SAE and ISO [8].

The mentioned origin coordinate system is located at the center of the contact interface between the road and the tire. The Z axis points downward and is perpendicular to the ground plane. The X axis is the interaction of the ground plane and wheel plane with the positive direction pointed to the direction of motion. Finally, the Y-axis direction is chosen in a way that the coordinate system is orthogonal. As a result, it is located in the ground plane and points to the right of the wheel plane. The forces and moments are generated along all axes directions during the operation of the tire. These forces and moments are caused by the interaction of the tire with the road surface and suspension inputs.

The applied forces to the tire are:

- F_x: attractive (or longitudinal) force;

- F_y: lateral force;

- F_z: vertical force.

The moments are:

- M_x: overturning moment;

- M_y: rolling resistance moment;

- M_z: aligning moment.

Using this coordinate system, we can define the performance parameters of the tire. For example, the traction/braking force is calculated by integrating the longitudinal shear stress over the tire contact interface. Additionally, the driving/braking torque over the tire's axis of rotation produces a force for accelerating/decelerating the vehicle. The generation of the tire forces may come from different sources. For example, the tire longitudinal forces are a resultant of the longitudinal friction force, thr tire rolling resistance force, and the longitudinal reaction force [7].

2.3   Rolling resistance

Rolling resistance is a dissipative force generated due to the rotation of the tire. During the rolling of the tire on a surface, the tire carcass repeatedly goes under deflection. Due to the hysteresis in the tire materials, the loading-unloading process of the tire structure dissipates energy, which accounts for a part of the rolling resistance on the tire. The circulation of the air inside the tire chamber and the flow of the air over the tire are other factors that impose drag forces on the tire. Additionally, during the traction/braking phase, the normal stress distribution in the contact patch shifts forward/backward relative to the tire YZ plane. Consequently, the normal force from the ground will produce a negative/positive moment around the Y axis that resist the accelerating/decelerating [7].

2.4   Rubber friction

Friction is a fundamental physical phenomenon, since it's a product from the contact of two bodies in relative motion. Thereby, the nature of frictional pairings is crucial for the description of dynamic contact problems in order to move one material against another.
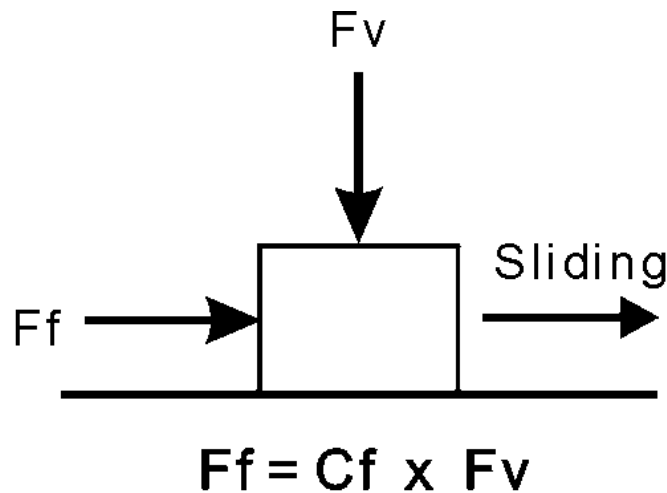
Figure 2.2: Friction coefficient [9]

The equation provided in the Figure 2.2 states that the force necessary to move a surface at a constant velocity on another surface is the product between the friction coefficient and the normal force (in this case is the weight of the block). For the same material, the static coefficient of friction is typically larger than the kinetic coefficient of friction. This means, that to move an object it will need a higher force than what is necessary to keep the object moving at a constant velocity [10, 9].

The prediction of traction properties of tyres under dry and wet conditions based on laboratory data still remains a difficult task. The main problems are the strongly non-linear behaviour of the rubber and the complex analytical description of dynamic contact

conditions between elastomers and rigid rough substrates.

In the literature [9, 10], mainly three mechanisms are considered to contribute to rubber friction:

- adhesive: interaction of interfacial layers that depends on the surface free energy of the bulk rubber and the rigid surface;

- deformation: arising from the deformation of the rubber by surface asperities;

- tearing wear: tearing of the rubber inner molecular bonds, which leads to tire friction.

These components of the friction force are shown in the Figure 2.3 below:
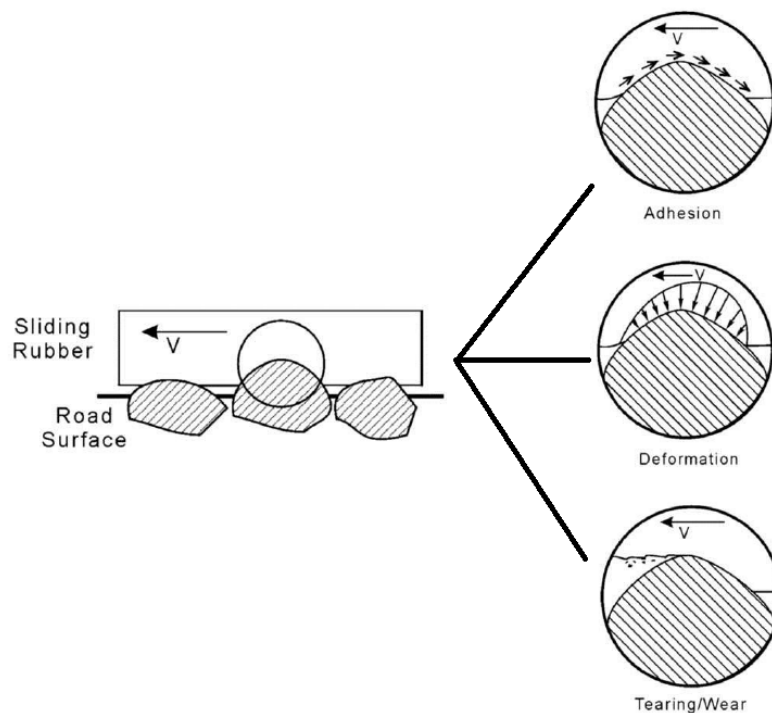
Figure 2.3: Major mechanisms involved in generation of the friction between rubber and terrain [9]

2.4.1 Rubber adhesion

The rubber adhesive properties are due to the Van der Waals intermolecular bonds between two surfaces. The adhesion is the main contributor to the friction force. The adhesion force magnitude depends on the area of the contact interface between the two objects, which is a function of the surface geometry, the contact pressure and the material properties [9].
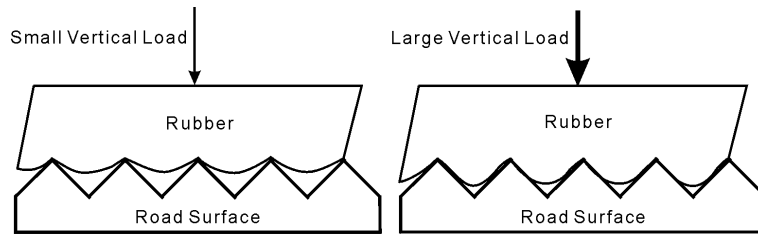
Figure 2.4: Increasing vertical load leads to a larger contact area [9]

As can be seen in Fig. 2.4, when the load is increased, the are of contact enlarges as a result of the surface irregularities penetration in the rubber. Thus, higher contact area leads to a higher friction.

2.4.2   Rubber deformation

Another force mechanism in the generation of friction is related to the rubber deformation (mechanical keying). As the tire surface slides over the road surface, the peaks of road irregularities (asperities) penetrate into the rubber surface. When rubber molecules drape over these asperities, a negative stress distribution, as shown in Figure 2.5, is generated at multiple contact regions that ultimately increases the vertical force (friction force).
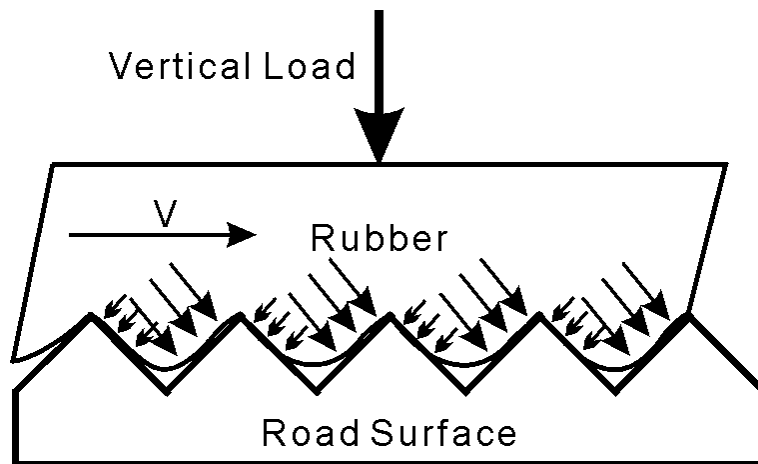
Figure 2.5: Mechanical keying [9]

2.4.3   Tearing and wear

Another mechanism of energy dissipation (friction), as a result of the rubber contact with a surface, is the traction forces produced by tearing and wear of the rubber. Tearing and wear is generated when the rubber sliding velocity increases at the location of sharp irregularities. Once the local stresses, located on the sharp irregularities, exceed the tensile strength of the rubber, the internal polymer bonds and crosslinks fail, causing the deformation beyond recover and a posterior disintegration of the rubber wear. The seperation of the rubber material (desintegration), in other words, wear, is the ultimate result of tearing [9].

2.5   Tire models overview

Due to the multiplicity and diversity of factors involved in the pavement tire interaction process, the analysis models tend to simplify the characteristics of the pavements, or the characteristics of the tires, as they are designed, on the mechanical engineering or civil engineering side respectively. However, more wide-range tire-pavement interaction models involving the main characteristics of the vehicle and the pavement are possible and, a must, in order to face the new challenges of the automobile industry, the construction and management of road infrastructure and the last and not least, emission control.

The tire model is selected regarding the scope of the study, the available computational resources, as well the the experimental resources, since some models need empirical data [11]. There's not a single tire model that can be used for studying the tire response in all sorts of loading scenarios and operating conditions. These models can be mainly grouped into three main categories:

- empirical models;

- physics-based models; and

- semi-empirical models.

2.6   Empirical models

The empirical models use the experimental data of the tire response and correlate it to the system parameters trough mathematical equations. These models are simpler tools for evaluating the the vehicles performance in similar environment conditions and tire properties. Since the parameters are calibrated for a certain test environment and tire properties, the results cannot be extrapolated to conditions outside the scope of the experimental data, resulting in a highly limited model. One of the most famous empirical models is the Magic Formula Tire Model, presented by Pacejka [12].

2.6.1   Physics-based models

Physics-based models integrate the physical principles and analytic methods to simulate tire structures and its interaction with the pavement. This models incorporates applied mathematics, numerical analysis and even computational physics to evaluate the performance of the vehicles. The complexity varies from the simple models that consider tire as a cylinder, a membrane, or a revolution shell to detailed models that use finite element formulations for tire characterization.

2.6.2   Semi-empirical models

The semi-empirical models are a mixture of the empirical and physics-based models, since it combines experimental measurements, empirical formulations and analytic methods to model the tire-road interaction. Using such hybrid models reduces the computational effort, making the semi-empirical tire models good candidates for full vehicle simulations in all sorts of conditions. However, since this model incorporate empirical correlations, the limitations of the empirical models prevails.

2.7   The archard wear model

The adhesive Archard wear model was introduced by Holm and Archard in 1953, and it's one of the most widely used wear model, mainly because of its straightforward application.
The model assumes that the area of contact is a sum of all areas of the contact surface profile peaks. The contact area, ΔA, is equal to πa^2 , where a is the radius equal to the contact point of the profile peak where the plastic deformation occurred. For a contact point, the contact pressure is changed to a contact force, which means that for this case the contact force in this case, is equal to the hardness of the softer material, and therefore [13, 3],

$$H = \frac{\Delta F}{\Delta A},\tag{2.1}$$

where, k is the probability that a particle will leave the system, once the asperity slides over the entire profile peak diameter ($2a$). When the particle leaves the system, it has overall volume (ΔV) of $2\pi a^3/3$, since it has a radius equal to a. Then the wear volume per sliding distance (ΔW), is [13, 3],

$$\Delta W = k\frac{\Delta V}{\Delta L} = k\frac{\pi a^2}{3}.\tag{2.2}$$

Substituting the equation 2.1 into 2.2 and introducing k=K/3, the total wear volume for a sliding distance s, is equal to [13, 3]:

$$V_T = W \cdot s = k\frac{F}{H}s.\tag{2.3}$$

2.8   Archard wear model for the Finite Element model

Based on Archard wear model the equation for calculating wear on each node on the tire tread can be developed according to equation 2.3, and, since $F = P \cdot A$. Substituting in the Equation 2.3, we end up with the general equation for finite element tire wear calculation for implementation in a programmed subroutine in Abaqus [3]:

$$V = k \frac{P \cdot A}{H} s. \tag{2.4}$$

Slip distance s is the product of slip rate $\dot{\gamma}$ and time t, then the material loss is:

$$\dot{V} = k \frac{P \cdot A}{H} \dot{\gamma}. \tag{2.5}$$

First, consider an entire outer surface of a tread ribbon, around tire in the peripheral direction, then the centerline of this surface is defined by a continuous sequence of nodes. The entire tread ribbon surfaces constitute the entire tread surface of the tire. The ablation process is expected to occur uniformly over the ribbons,

$$\dot{V} = \frac{k}{H} \int_{ribbon} P(x,t)\dot{\gamma}(x,t)\mathrm{d}A, \tag{2.6}$$

where x is the configuration position at described time t. For simplification purposes, a time-independent form is chosen since a steady-state transport code is used, which is based on an Eulerian steady-state transport. Also, ignoring the variation in stream ribbon width and the contact areas (since its a nodal contact), the ablation rate comes in the following form,

$$\dot{V} = \frac{k}{H} \int_{s} P(s)\dot{\gamma}(s)T(s)\mathrm{d}s, \tag{2.7}$$

where s is the position along the streamline and $T(s)$ is the width of the stream ribbon at position s.

Expressing the Equation 2.7 as a function of the local material ablation rate, it comes in fowling form:

$$\dot{V} = \int_{s} \dot{h}(s)T(s)\mathrm{d}s. \tag{2.8}$$

Discretizing the Equations (2.7) and (2.8) simultaneously, the wear rate equation as:

$$\dot{h} = \frac{k \sum_{n=1}^{N} P_n \dot{\gamma}_n \Delta S_n}{H \sum_{n=1}^{N} \Delta S_n}. \tag{2.9}$$

2.9   Abaqus adaptative mesh control

In order to simulate the change in the tire geometry due to the ablation, an Arbitrary Lagrangian-Eulerian (ALE) adaptive mesh domain must be defined. Abaqus/Explicit provides a general and robust adaptive meshing capability for problems ranging from quasi-static to dynamic. The ALE adaptive meshing is implemented through the adaptive mesh domains option, which can be either Lagrangian or Eulerian.
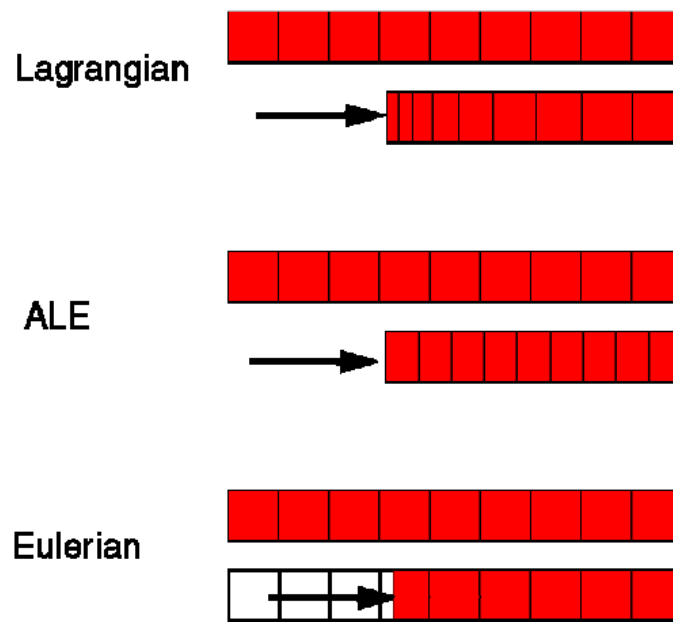
Figure 2.6: Mesh motion under different mesh constrains [14]

- Lagrangian mesh constrain: most problems in Abaqus use a pure Lagrangian description, where the mesh moves attracted to the material. One of the big advantages of using a Lagrangian approach is that it is easy to track free surfaces and to apply boundary conditions. However, the mesh will become highly distorted when under high strain gradients;

- Eularian mesh constrain: contrary to the Lagrangian adaptive mesh, the nodes are fixed in space while material flows through the mesh, making this mesh constrain most suitable for analyze of steady-state processes involving material flow. Furthermore, material can flow into or out of the mesh on certain boundaries;

- ALE mesh constrain: this is a tool that combines the features from the previous described mesh constrains types. It maintains a high-quality mesh throughout the analysis, regardless of material loss. ALE mesh constrain allows more complex contact interactions and more accurate definition of the boundaries of the material, being the recommended tool to model the effects of the wear on a tire tread, in which material is eroded at the surface [14].

2.10   Tire structure components

A modern typical tire is manufactures from nearly 10-25 different components. A simplified view from the tire sections of a typical radial passenger car tire is shown in Figure 2.7. The tire individual parts are created by rubberizing different components including cables, textiles and steel belts with rubber compounds. These components are assembled on the tire assembly machine into an elastic green tire. Then, tire goes through the vulcanization process in order to become a unique part. During the curing process, high pressure steam is conducted into the vulcanization pad inside the vulcanization press, and pushes the tire components against the walls of the molds. Finally, the tread pattern and side texts on the tire sidewall are created [15].
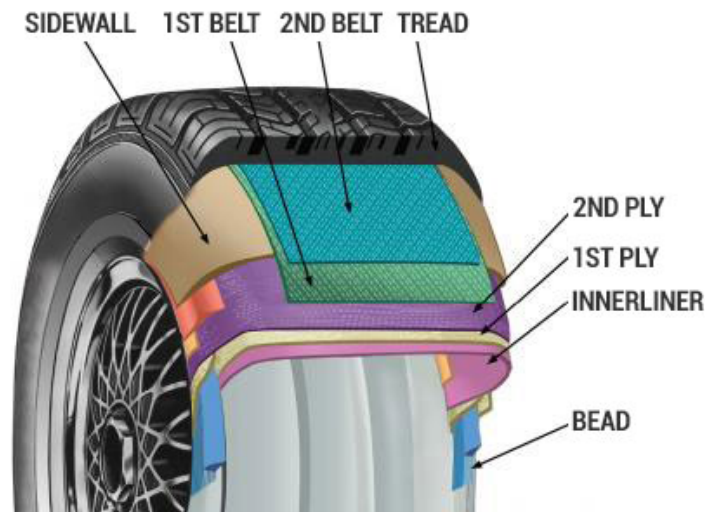
Figure 2.7: Tire elements [16].

The main structural components, that significantly contribute to the tire structural dynamic and response characteristics, are identified as follow:

- tread - ensures high mileage, good road grip and water expulsion;

- 1st belt - optimize directional stability and rolling resistance;

- 2nd belt - enables high speeds;

- 1st ply and 2nd ply - controls internal pressure and maintains the tyre's shape;

- sidewall - protects from external damage;

- innerlinner - makes the tyre airtight; and

- bead - promotes directional stability and precise steering response, promotes directional stability and steering performance and comfort level.

2.11   Hyperelastic materials

A great portion of the tire structure consists of vulcanized elastomers such as rubber material. Rubber has a nonlinear and incompressible behavior toward loading, which is independent of the strain rate and belongs to a type of materials name "Hyperelastic". An hyperelastic material differs from the well known elastic material in three main aspects [17, 18]:

- hyperelastic materials are almost incompressible, keeping their volume during loading. Furthermore, hyperelastic materials can be subject to large deformations and still recover their initial shape;

- hyperelastic materials such as rubber show higher stress magnitude in compression in comparison with tension, for an identical strain magnitude;

- finally, hyperelastic materials exhibit a stiff response, i.e., when subjected to tension, it softens and then become stiffer again.

There are many models that describe the behavior of an hyperelastic material based on strain energy functions, by predicting the stress-strain relationship. The most well established models are the Neo-Hookean model, Yeoh, Marlow, Ogden and Gent Stress-strain curves for a variety of hyperelastic material models are shown in Figure 2.8.
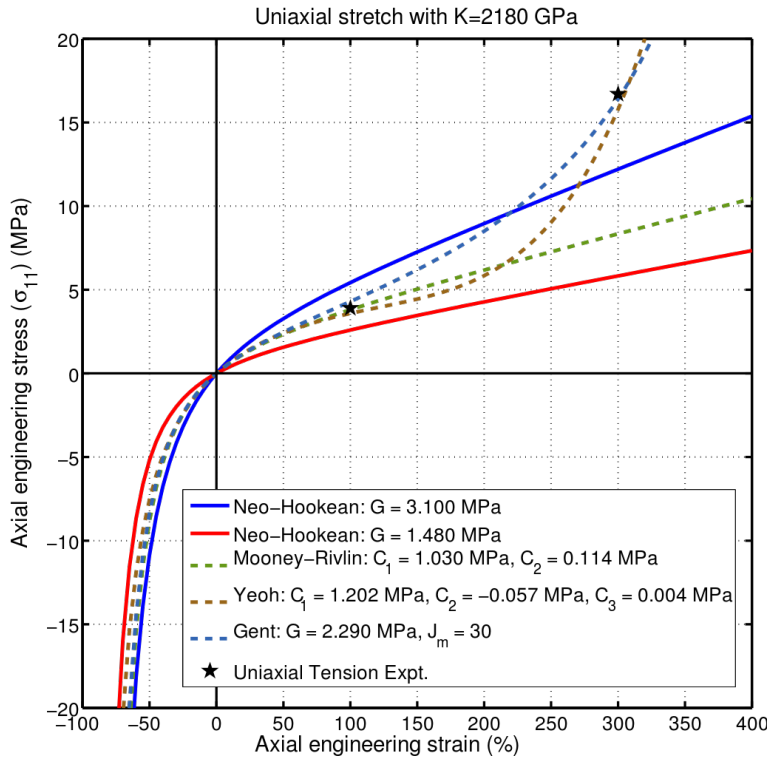
Figure 2.8: Stress–strain curves for various hyperelastic material models[19].

2.11.1   Neo-hookean model

The neo-hookean model is similar to Hooke's law, being well established for the study of the vulcanized rubber,

$$W = C_1(\bar{I}_1 - 3) + \frac{1}{D_1}(J^{el} - 1)^2, \tag{2.10}$$

where C_1 is the material constant, defined by $\mu_0 \frac{1}{2}$ (μ_0 is the initial shear modulus of the material), $\bar{I}_1$ is the first invariant of the left Cauchy-Green strain tensor and D_1 is temperature-dependent material parameters [20]. Examining the Neo-Hookean curves of the Figure 2.8, it can be seen that the material will initially be linear until a certain point. From there, the curve tends to flatten, mainly due to to the release of energy as heat while on heavy stresses. This is a typical behavior of an hyperelastic, or rubber like material, and its due to the fact that when a stress is applied, the polymer cross-linked chains can move relativity to each other until a certain stress levels, after what the elastic modulus of the material increases dramatically [21, 20, 22].

2.11.2   The Mooney-Rivlin model

The Mooney–Rivlin model for rubber-like materials is a hyperelastic material model developed by the same researchers has the Neo-hookean model, Ronald Rivlin and Melvin Mooney. In this hyperelastic model, the strain energy density function W, is a linear combination of two invariants of the left Cauchy–Green deformation tensor [21, 20, 22]. The strain energy density function is defined as follows:

$$W = C_1(\bar{I}_1 - 3) + C_2(\bar{I}_2 - 3) + \frac{1}{D_1}(J^{el} - 1)^2, \tag{2.11}$$

2.11.3   Yeoh model

The Yeoh hyperelastic model, also called the reduced polynomial model, for incompressible rubber-like materials, was proposed in 1990 by Yeoh, and is based on the first strain invariant:

$$W = \sum_{i=1}^{3} C_{i0}(\bar{I}_1 - 3)^i, \tag{2.12}$$

where C_{i0} are material constants and $\bar{I}_1$ is the first invariant of the left Cauchy-Green deformation tensor[20]. The initial shear modulus comes as C_{i0}. When $i = 1$, the incompressible Yeoh model reduces to the Neo-Hookean model for incompressible materials [21, 20, 22].

In the presented work, the material properties were assigned based on the Yeoh hyperelastic model. The material constants came from the work presented by Palanivel et al. [2] and applied directly in the Abaqus tire model. The tire material properties are presented in Table 2.1.

Yeoh model material constants					
Components	**Density** (kg/m^3)	**C10**	**C20**	**C30**	**D1**
Inner linner	1050	3.14470e5	-1.10385e5	2.65448e4	1.58998e-7
Ply	1050	3.72454e5	-9.69403e4	2.43385e4	1.34244e-7
Belt	1050	8.96732e5	-2.80203e4	7.88071e4	5.57580e-8
Filler	1050	8.76048e5	-2.93303e5	7.93587e4	5.70745e-8
Sidewall	1050	4.87666e5	-1.41343e5	3.86106e4	1.02529e-7
Shoulder	1050	6.16047e5	-1.90709e5	4.75049e4	8.11627e-8
Rimstrip	1050	1.13364e6	-4.43953e5	1.18935e5	4.41059e-8
Tread	750	6.16047e5	-1.90709e5	4.75049e4	8.11627e-8
		Young's modulus		**Poisson**	
Bead	7800	2.06399e11		0.3	
Reinforcement definition of geometry					
	Cross sectional area of rebar (m^2)	**Spacing between rebar** (m)		**Orientation angle** (degree)	
Ply	3.52565e-7	9.056e-4		-1	
Belt 1	1.41196e-7	1.581e-3		60	
Belt 2	1.41196e-7	1.581e-3		-60	

Table 2.1: Yeoh model material constants [2].

Part II

Methods and Models

Chapter 3

Abaqus tire modelling

3.1 Introduction

The tyre is a complex structure with a lot of different components, every component (either a cord reinforcement or a rubber compound) has a specific task in the final structure [1].
The tread is the direct connector between the vehicle and the road, his compound material properties having to achieve a long lifetime of the tyre and his damping properties having to guarantee good traction and braking results. The cap ply is a textile cord directed into circumferential direction. This reinforcement has big influence on the dynamic contour, which has direct correlation to the high speed durability. The two steel belt layered package (with same positive and negative angle against the circumferential direction) is the most important component in the tyre to achieve the necessary stiffness. To get the final shape of the tyre, all components are heated during the production process within a mold.

3.2 Abaqus cross-section tire model

A passenger car, radial tyre, of size 205/55R16, has been chosen to construct the axyssimetric finite element model, which has the same size as used by Palanivelu et al. [2]. The finite element modeling starts with a draw of the axysimmetric section of the tire in Abaqus (Figure 3.1). In this study, to keep the model relatively simple, the detailed geometrical sections of the tire, such as the two ply sections, were not considered. Instead, it was just considered one section, based on figure 2.7, which is already a conservative approach to tire components.
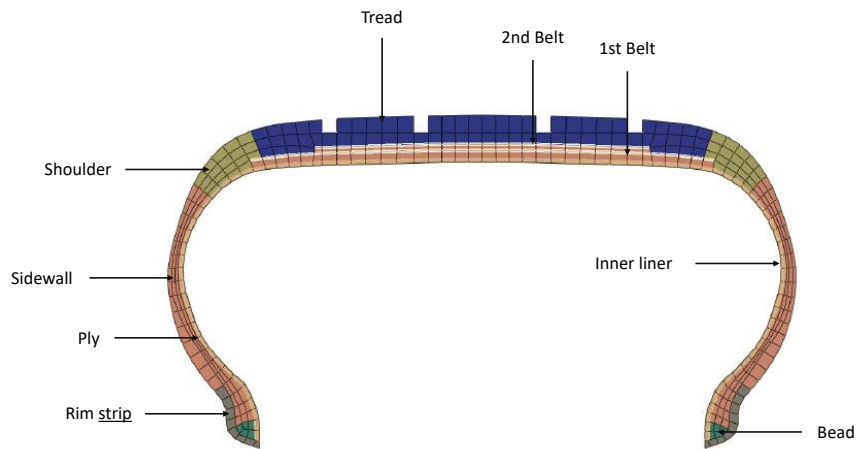
Figure 3.1: Abaqus axysimmetric tire model

Both belts and ply are modeled as surfaces for further assignment as rebar layers for reinforcement purposes. Using this approach allows for the mesh of the reinforcement sections being independent of the host elements, avoiding unwanted meshing problems. Hyper-elastic Yeoh model was used to define the material properties, as it approximate the real behavior of the tire, with proven results in Palanivelu's *et al.* work [2].

The elements used in the axyssimetric model are SFMGAX1 for reinforcements (145 elements) and CGAX4 elements for the rest of the model (433 elements), totalizing 578 elements and 529 nodes.

From the 2D axysimmetric section, the tire was revolved into a 3D model (Figure 3.2) by means of an Abaqus function *SYMMETRIC MODEL GENERATION with general elements option.
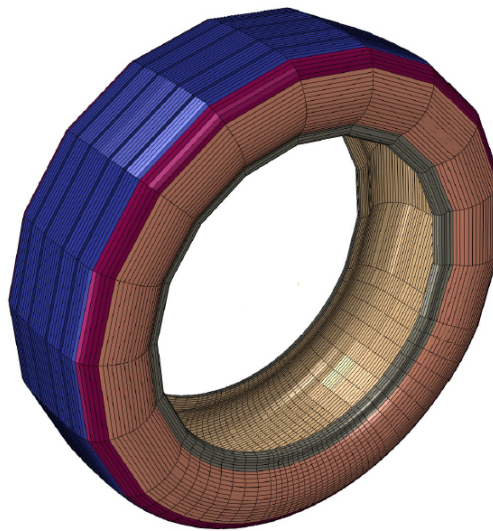
Figure 3.2: 3-D Finite Element tire model.

The revolve operation converts all SFMGAX1 elements to SFM3D4R (surface elements) and therefore CGAX4 elements to C3D8 3D solid finite elements. In order to reduce computation time, the mesh starts on the top of the tire with a coarse mesh and gets finer as long as it approaches the first contact node between the tire and pavement.

3.3 Road modelling

In order to simulate the tire-road interaction, the road is considered as an analytical rigid surface, and a surface-to-surface contact interface is established between the tire tread and the road. The zero-gap contact is achieved by modeling the contact problem using a Lagrange multiplier method, combined with 4 coefficients of friction that will be tested in the present work: 0.8, 1.0, 1.1, 1.3. The Lagrange Multiplier method satisfies the contact boundary condition more accurately than other methods, such as the Penalty method.

3.4 Summary

The procedure for developing a full finite element tire model starts with the implementation of the geometrical properties of the tire section (axysimmetric cross section) into Abaqus software, and assigning to it the proper material models and coefficients. Then, the fully defined section model is modeled using proper FEM elements, using a quad element shape with medial axis algorithm. Next, the individual section is revolved into a 3D tire model. Finally, proper contact models are assigned to corresponding sections interfaces (reinforcement layers), in order to model the interaction of the tire components with each other as well as the tire with the road.

Intentionally blank page.

Chapter 4

Abaqus FEM modelling

4.1 Introduction

In order to study the transient behavior of the tire using Abaqus Finite Element software, preliminary verification and validation exercises should be carried out. Here, verification is the process of evaluating the model implementation to make sure that it does not have any error or programing mistakes. In this regard, the stability and convergence of the model implicit and explicit solvers are examined initially throughout various simulation stages. The validation study is the process of evaluating to which extent the developed model can represent the real structure. For this purpose, a series of simulation case studies are considered in order to examine the tire model response characteristics in static and dynamic conditions. Then, the simulation results from these steps are compared to the empirical data from experiments with identical system inputs, and subsequently the accuracy of the developed model is discussed.

4.2 Simulation case studies

The finite element analysis of the tire simulations can be categorized as implicit or explicit[23]. The implicit methodology uses an iterative approach, in addition to an Newton-Raphson algorithm in order to construct and update the mass and stiffness matrices while enforcing the equilibrium at the end of each step. This method is used for solving the preliminary steps in Abaqus/Standard prior to the dynamic transient simulations.
These steps consist of inflating the tire with simulated rim constraints, bringing the tire near the surface, performing loading analysis and steady-state rolling.
Subsequently, the transient behavior of the tire in simulations (such as traction and rolling) was captured using an explicit approach. The following simulations have been performed in this study are the following:

- tire inflation of 220 kPa - friction coefficient values of: 0.8, 1.0, 1.1, 1.3

- tire inflation of 240 kPa - friction coefficient values of: 0.8, 1.0, 1.1, 1.3

- tire inflation of 250 kPa - friction coefficient values of: 0.8, 1.0, 1.1, 1.3

- tire inflation of 280 kPa - friction coefficient values of: 0.8, 1.0, 1.1, 1.3

- tire inflation of 300 kPa - friction coefficient values of: 0.8, 1.0, 1.1, 1.3

An overview of simulation setup procedure is shown in Figure 4.1

Step 1 (Implicit)
- **Axysimmetric model Generation**
  - Assign of: Section properties, material properties;
  - Definition of mesh properties ;
  - Inflation of the axisymetric model.

Step 2 (Implicit)
- **Tire Static Footprint Analysis**
  - Transfer tire inflation results from the step 1 and 3D generate model using *SYMMETRIC MODEL GENERATION;
  - Bring transferred axisymmetric results to equilibrium;
  - footprint analysis (displacement control);
  - footprint analysis (load control);

Step 3 (Implicit)
- **Steady state simulation**
  - Simulation of a rolling tire.

Step 4 (Explicit)
- **Steady-state transport analysis**
  - Implementation of a fortran subroutine for wear simulation.

Figure 4.1: Abaqus simulation steps procedure.

4.3   Tire static footprint analysis

In order to obtain the simulation prediction of footprint of the tyre, the analysis is divided in three distinct steps. In the first step, tire inflation (220, 240, 250, 280, 300 kPa) occurs. In the second step, the contact between the tire and the road starts with a road displacement (with a null friction coefficient). The script for the full analysis is given in the Appendix A for a better insight. The second step is based on the script provided by Abaqus on the study of the tire tread wear [18]. In the third step (the last one of the static analysis) a load of 6000 N is imposed in order to simulate the weight in a single front tire. The simulated weight used in the analysis match the weight of

an 2018 Audi A4, which has a weight distribution 60/40(f/r) and a gross vehicle weight around 2010 kg.

In the Figure 4.3, the static footprints of a tire with a simulated load of 6000 N are displayed, in order to better understand the static behavior of the tire when in contact with a road surface.
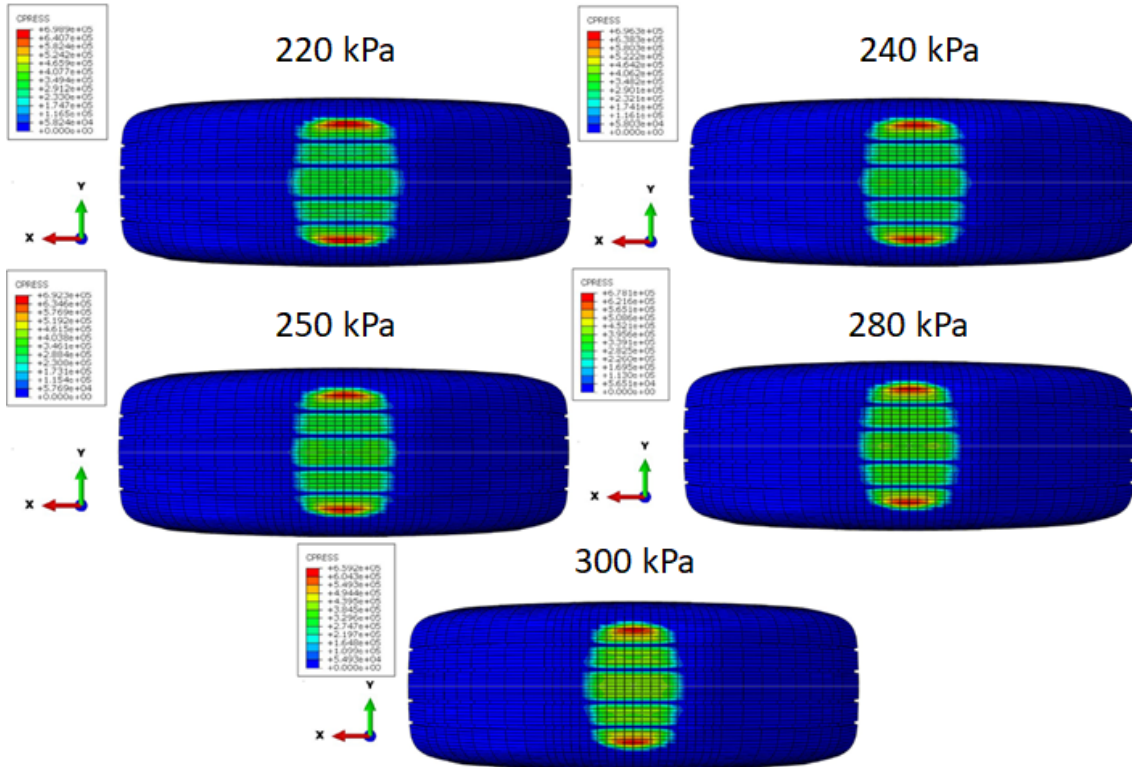
Figure 4.2: Static footprint under a 6000 N load, for incrementing inflation pressures.

The contact patches are very similar but, looking closely, as the pressure in the inside wall rises, the area of the contact patch tends to shrink, which will increase the normal force generated by the interaction tire-road. It can be concluded, according to Equation 2.5, that the inflation pressure and tread wear will vary accordingly as a direct proportion for the same wear coefficient.

In the next chapter, a more detailed analysis will be given, as the Archard wear model is used to quantify the tire wear under a cycle of 555,5 km.

Bearing in mind the results obtained in the paper presented by Palanivelu *et al.*[2] for the tire footprint, an analysis with the specified assigned properties was conducted in order to verify the robustness of the results presented in this work.
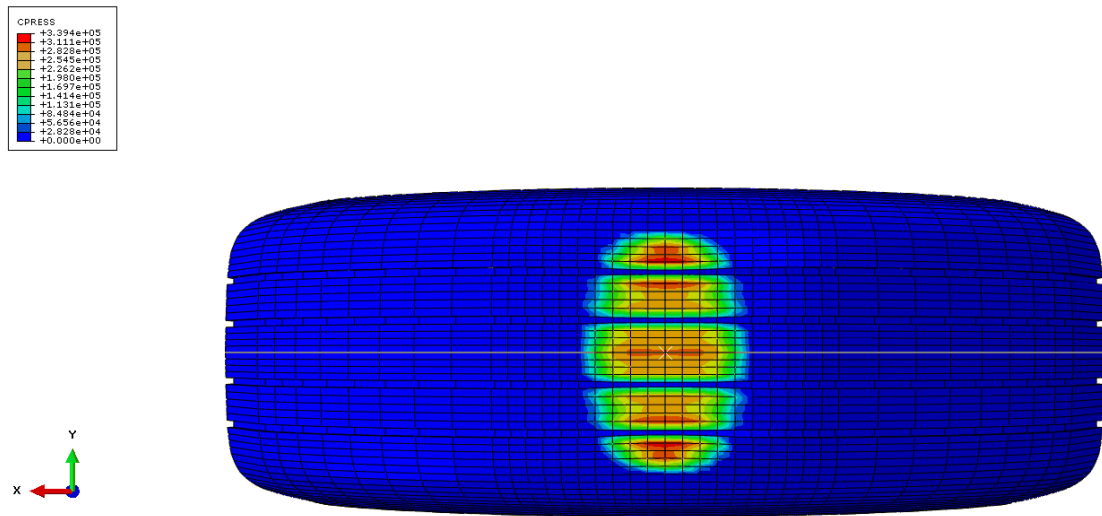
Figure 4.3: Static footprint under a 3000 N load, with a 250 kPa inflation pressure.

The contact patch lacks of an homogeneous distribution of the contact pressure, although the values for the maximum contact pressure are analogous. The discrepancy in the contact pressure distribution can be caused by many different factors, such as, distinct tread patterns and different refinement of the mesh. In the present analysis an implicit method was used, in contrast with the explicit method adopted by Palanivelu *et al.*. Finally, a different Finite Element are used in that work, although there is no reference to the specific Finite Element used to generate their 3D model.

4.4   Steady-state rolling analysis: straight rolling

Following the previous results, a detailed analysis of the contact patch while the tire is on rolling conditions, is explained in the next subsections, where are established four different road friction coefficients. Again, the analysis script is displayed on Appendix B for a better comprehension of the simulation process, and is based on the script provided by Abaqus on the study of the tire tread wear [18]. Furthermore, in order to run the Fortran subroutine in Abaqus 6.13, Visual Studio 2012 and the in Intel xe version 13 has to pre-installed.

4.4.1   Friction coefficient of 0.8

A friction coefficient of 0.8 is out of the reality nowadays, at least for passengers vehicles, since the common friction coefficients for a dry road is between 1.1 and 1.3 depending on the tire geometric and material properties. Nevertheless, simulations for a coefficient of 0.8 were conducted in order to have a term of comparison to others friction coefficients. In the following image (Figure 4.4), a comparison between the contact patches are undertaken in order to understand the behavior of the tread rubber under different inflation pressures.
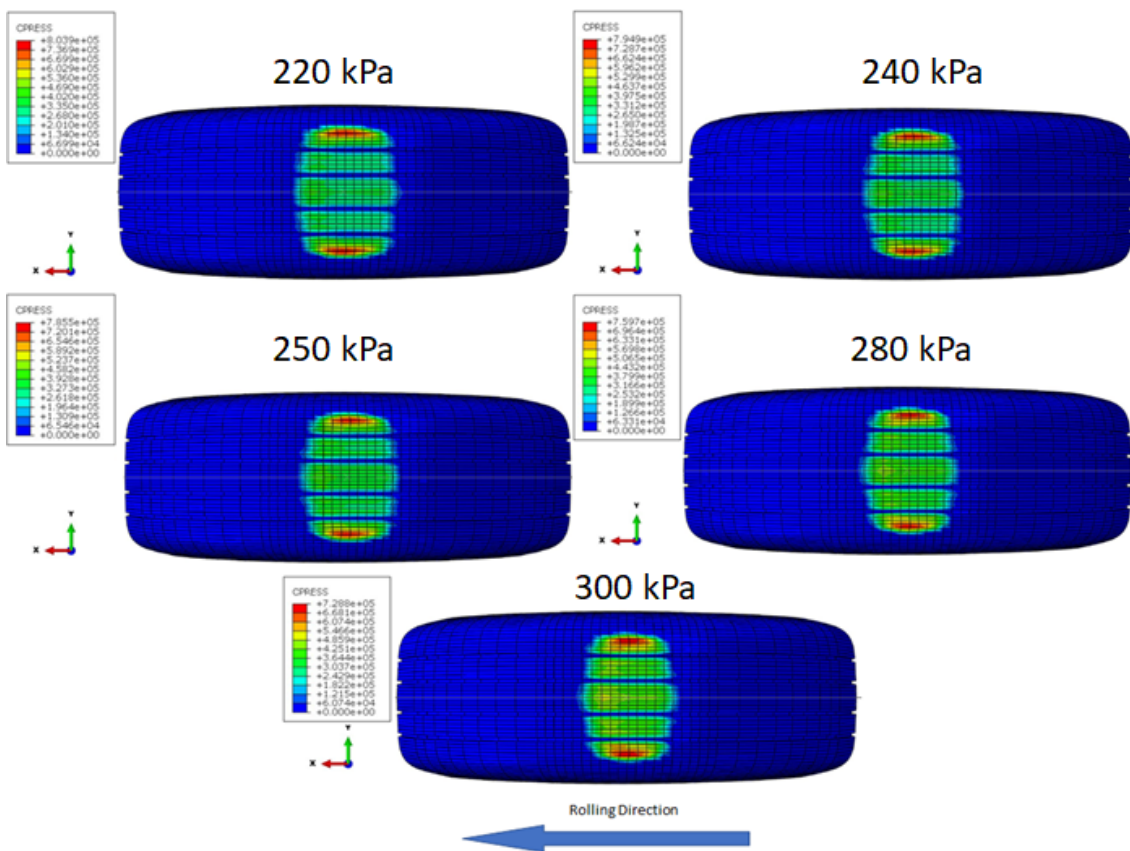
Figure 4.4: Straight rolling for a 0.8 friction coefficient.

From the Figure 4.4), it is clear the reduction of the contact area, as previously stated in the static footprint analysis of the tire behavior with the increase in the inflation pressure. As the tire goes from static to a rolling state, mainly due to the inflation pressure and, due to the viscosity's of the tread, the phenomenon of adhesion occurs, causing the appearance of accumulated pressure zones in the middle tread. This leads to conclude that, although the maximum contact pressure decreases as the the inflation pressures increases, the wear volume will be higher due to the newly created focus of tension.

4.4.2 Friction coefficient of 1.0

Following a more reasonable approach to the friction coefficient, the same tests were conducted with a friction coefficient of 1.0 instead of the previous 0.8. The results are shown in Figure 4.5:
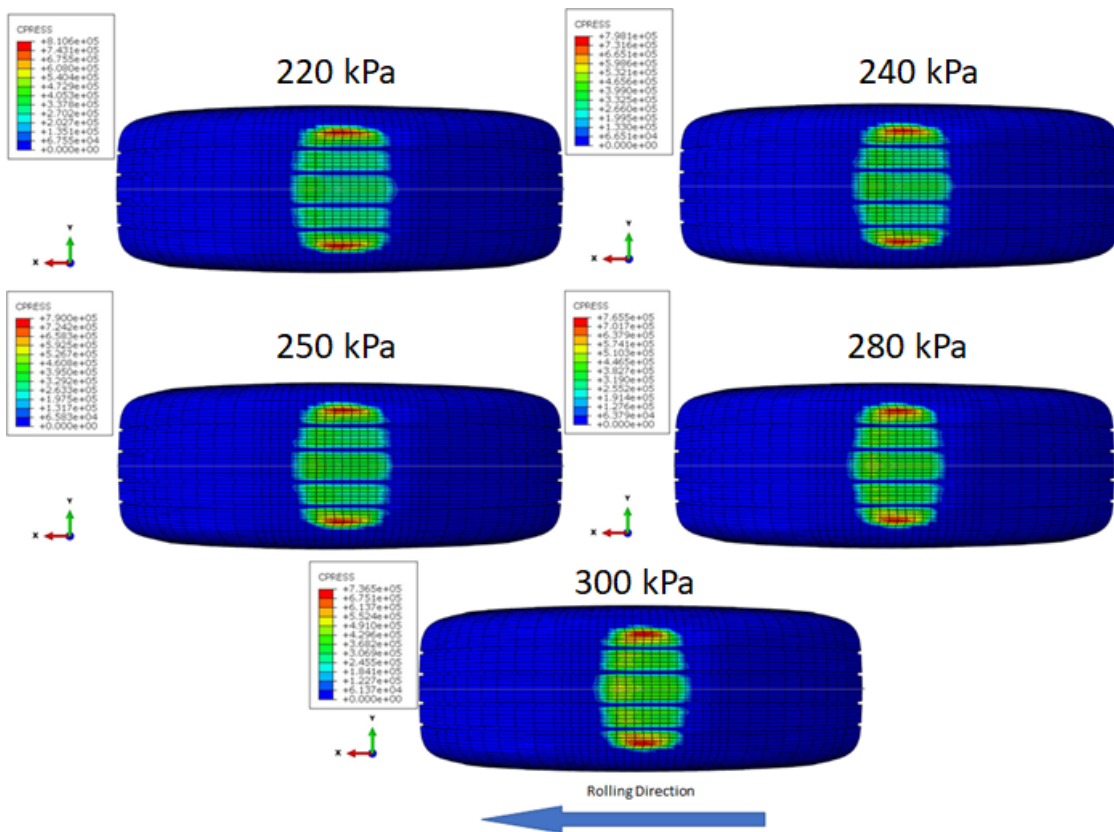
Figure 4.5: Straight rolling for a 1.0 friction coefficient.

Comparing Figure 4.5 with Figure 4.4, there are some visual discrepancy's. First, the contact pressure is slightly higher has compared to the contact pressures related to the friction coefficient of 0.8. Second, the adhesion phenomenon is even more visible as the tread starts to stretch along the contact interface tire-road. Finally, for higher pressures, the previous concentration of forces tend to spread.

In the next subsection the friction coefficient is increased to 1.1 for a better insight of the tire behavior change with higher friction levels.

4.4.3   Friction coefficient of 1.1

Changing into a friction coefficient of 1.1 that better fits into reality, the results are displayed in the figure below.
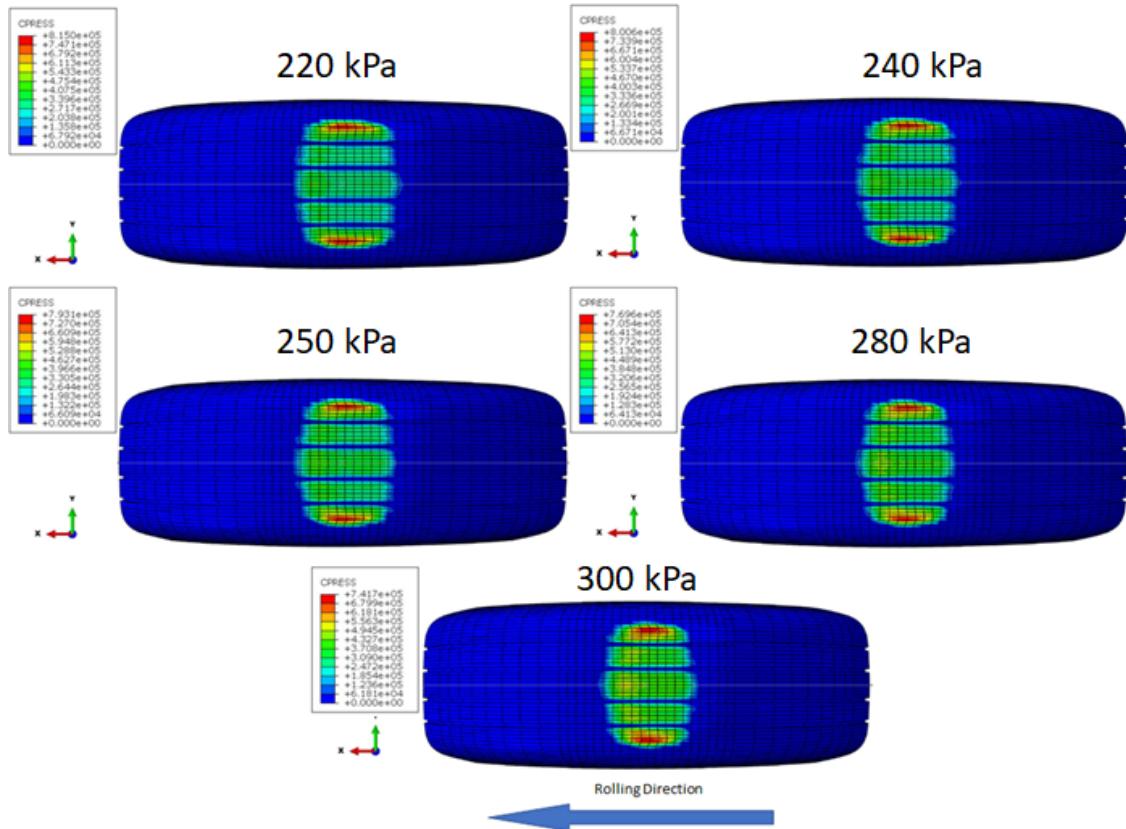
Figure 4.6: Straight rolling for a 1.1 friction coefficient.

The changes in the tire behavior are almost imperceptible, the only differences are the increase of the contact pressures in comparison with the Figure 4.5. In the next subsection the coefficient of friction is increased to 1.3 in order to get a deeper comparison with the previous friction coefficients and a even better approach to the reality.

4.4.4 Friction coefficient of 1.3

A final test was conducted with a friction coefficient of 1.3. The results are presented in the following image:
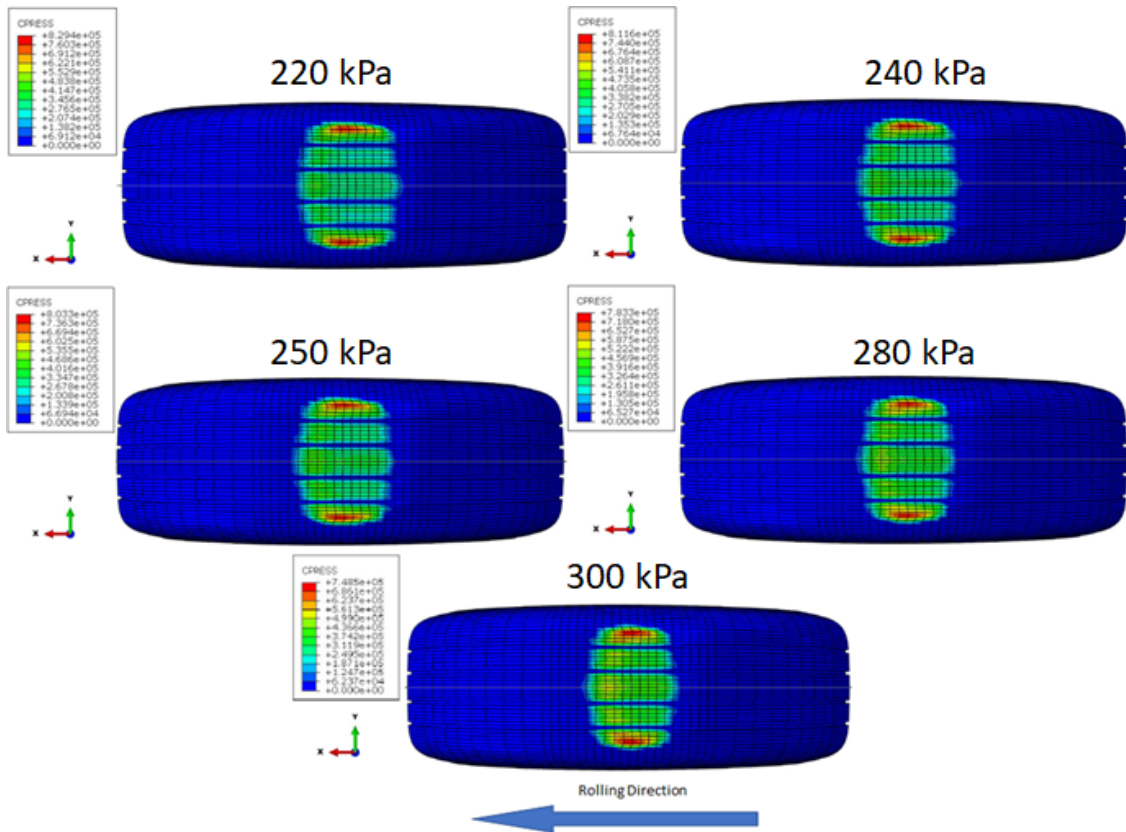
Figure 4.7: Straight rolling for a 1.3 friction coefficient

Comparing the previous figures, a correlation can be built with the presented results, and some conclusions can be taken for the relation between the inflation pressure and the friction coefficient.

First, for a constant friction coefficient and an increasing inflation force the contact patch area tends to retract, as well the contact pressure decreases. In the meanwhile, zones of concentrated pressure appear in the middle tread, mainly due to the phenomenon of adhesion. Second, isolating the pressure with a varying friction coefficient it can be concluded that the contact pressure increases with an increase friction coefficient, although the contact patch geometry remains the same.

The next step in this work, is to measure and quantify the wear in the different scenarios as stated before for both inflation pressure and friction coefficient.

4.5   Wear analysis

4.5.1   Wear implementation process

With the expression for wear rate in the form of a surface ablation velocity as stated in Equation 2.9, the wear simulation can now be applied in a steady-state transport analysis (Abaqus subroutine on Appendix C), together with the Fortran subroutine (Appendix D), which are both based on the scripts provided by Abaqus [18]. Subroutine UMESHMOTION is used to specify the ablation velocity vectors at the nodes of the exterior surface of the tread. The detailed Fortran subroutine can be found on Appendix D. The tire model is run for a duration of 50 000 seconds equivalent to a 555,6 km of operation at 40 km/h.

4.5.2   Wear analysis

In following images, the obtained results, coming from the implementation of the wear subroutine, are shown using a Lagrangian adaptive mesh control as previously explained in Section 2.9.

4.5.3 Friction coefficient of 0.8
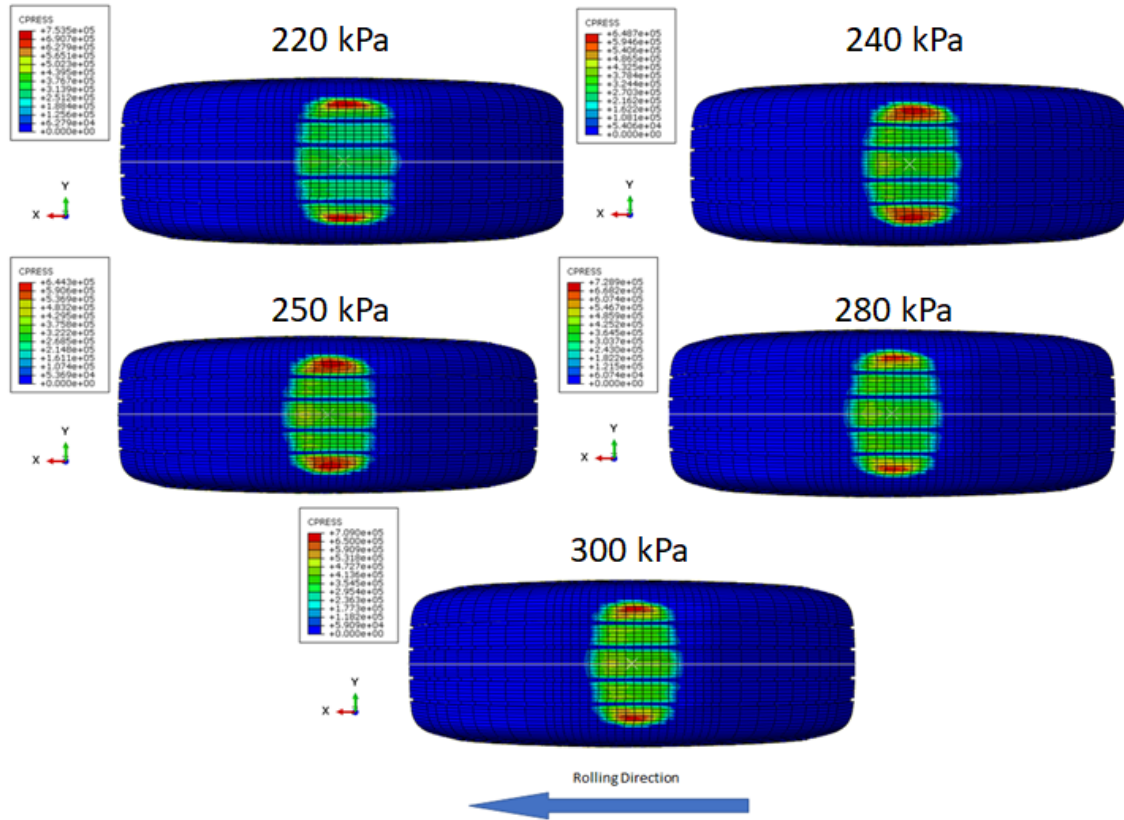
Figure 4.8: Worn tire contact patch for a 0.8 friction coefficient.

In comparison with the footprints from the Figure 4.4, the contact patch has a superior given area to the peak pressure distribution mainly due to the higher wear rate in outermost region of the tire contact patch. The contact pressure suffers a slight reduction since as the contact area increases, since the shape of tread region in the tire cross section tends to flatten. Furthermore, for tire inflation pressures of 280 and 300 kPa, the contact pressure distribution remains almost identical, which means the wear rate is similar in every node of the tire cross section in contact with the road.

4.5.4 Friction coefficient of 1.0
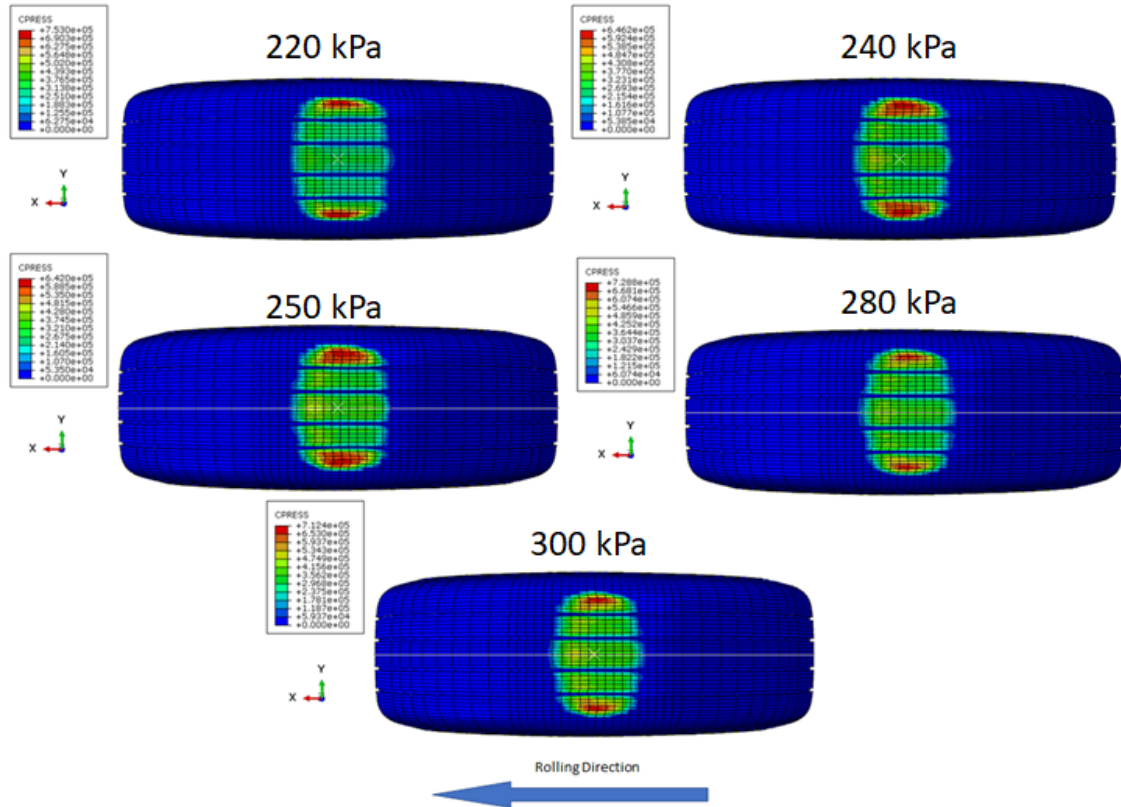
Figure 4.9: Worn tire contact patch for a 1.0 friction coefficient.

The ablation results with a friction coefficient of 1.0 leads to the same conclusion as stated in the previous subsection: the area from the contact patch increases as a result of the tire surface ablation resulting in a contact pressure drop.

4.5.5   Friction coefficient of 1.1
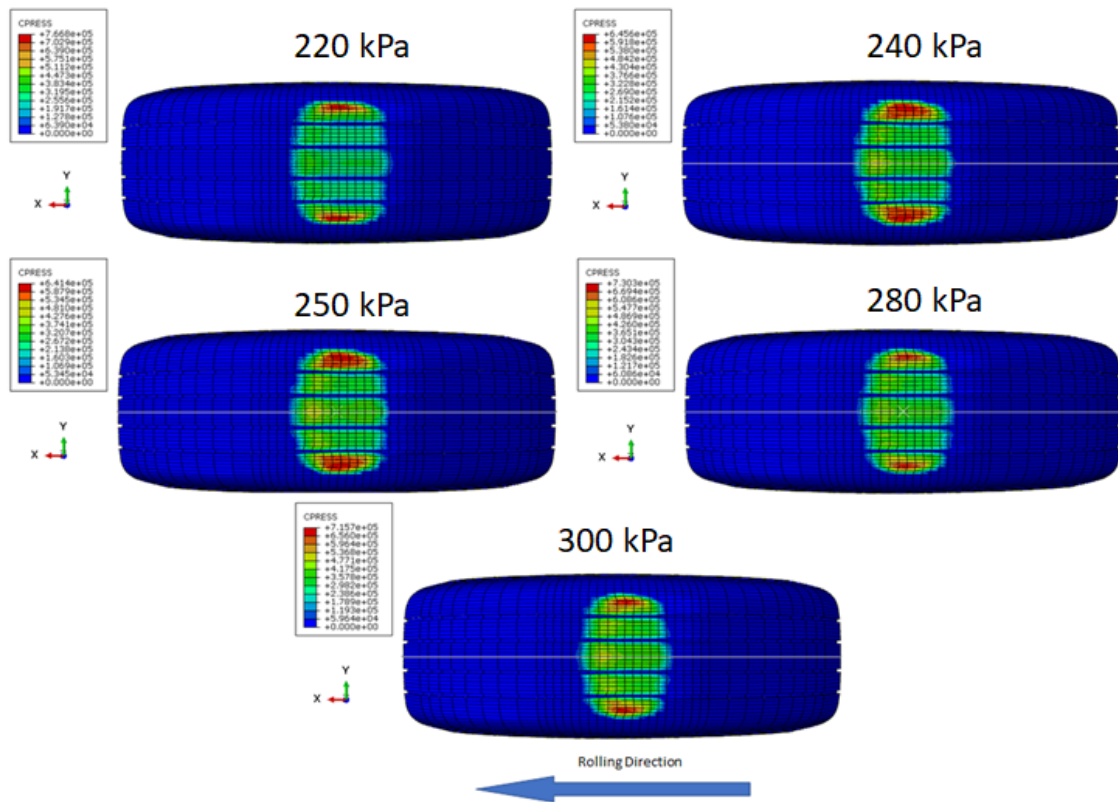
Figure 4.10: Worn tire contact patch for a 1.1 friction coefficient.

Again, for the analysis with a friction coefficient of 1.1, the tire patch continues to exhibit the same behavior as the contact patch of the tire bound to a friction coefficient of 0.8 and 1.0.

4.5.6 Friction coefficient of 1.3
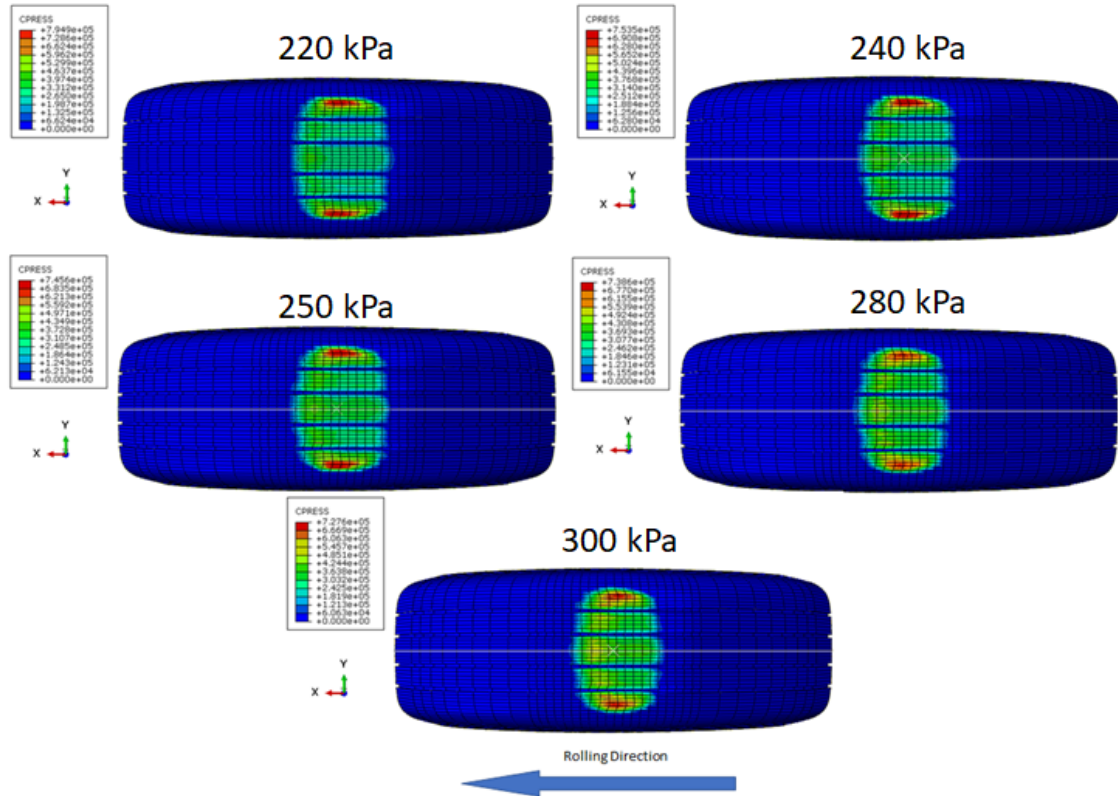
Figure 4.11: Worn tire contact patch for a 1.3 friction coefficient.

The tire behavior under rolling condition with a friction coefficient of 1.3, is identical to the ones with the previous friction coefficients, except for the pressures of 280 and 300 kPa. For the inflation pressures of 280 and 300 kPa the contact patch retracts as a result of a higher decrease in the tire outer diameter.

Intentionally blank page.

Part III

Results and discussion

Chapter 5

Results

As stated in the previous chapter, the wear analysis was carried out using a Fortran subroutine. The results were obtained by plotting the displacement of the node n°50 (Figure 5.1) which is a node on the plane that divides the tire in two symmetric parts in the longitudinal direction.
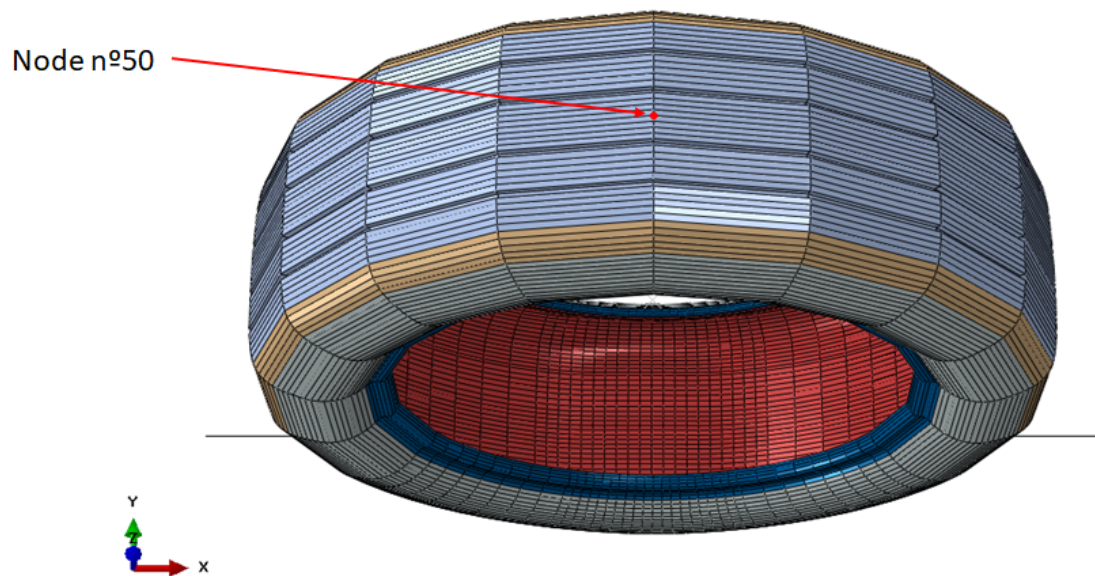
Figure 5.1: Location of the node used to extract the total wear on the tread after a cycle of 50 000 seconds

5.1   Wear depth vs pressure

As part of the wear analysis, five graphics (Figure 5.2, 5.3, 5.4, 5.5) with the correlation between wear depth and the tire pressure. The following correlations represents an attempt to develop a direct mathematical equation to predict tire wear, for the tire geometry previously described, according to the pressure and friction coefficient.
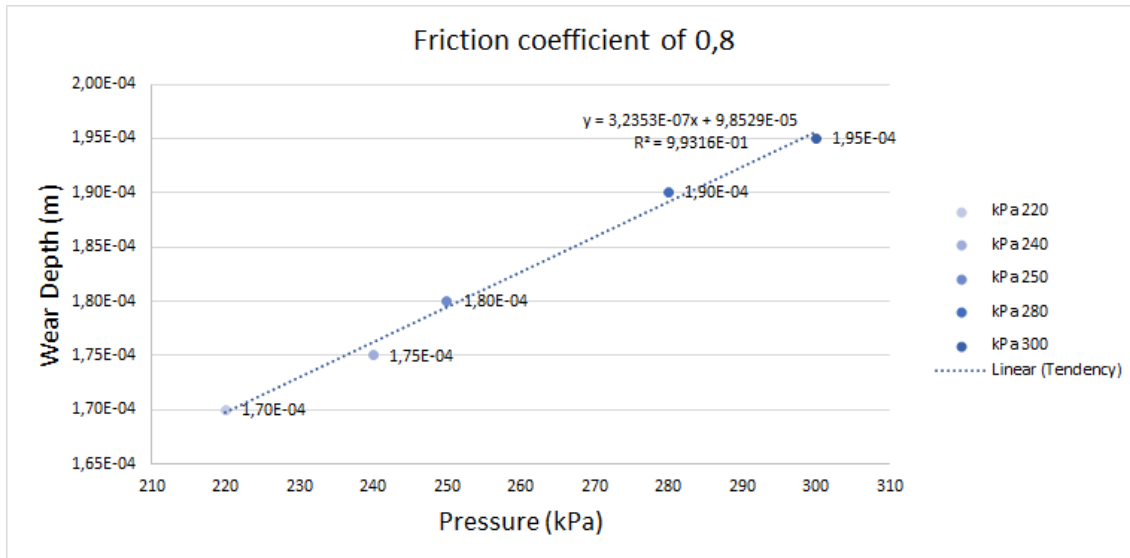
Figure 5.2: Wear depth in straight rolling with a friction coefficient of 0.8

According to the previous graphic (Figure 5.2), there is direct correlation between ablation and inflation pressure. Furthermore, higher pressures leads to a higher ablation rate. Following up the tendency line equation, and since the error is around 0,68%, it's possible to predict with a the wear depth for different pressures, substituting the variable x for the desired pressure in kPa. The extrapolation of the current results for a different rolling distance is not appropriate since, with the tire wear, the contact patch tends to enlarge which leads to a decrease in the heat dissipation (increase in frictional heating), thus, changing the wear rate.
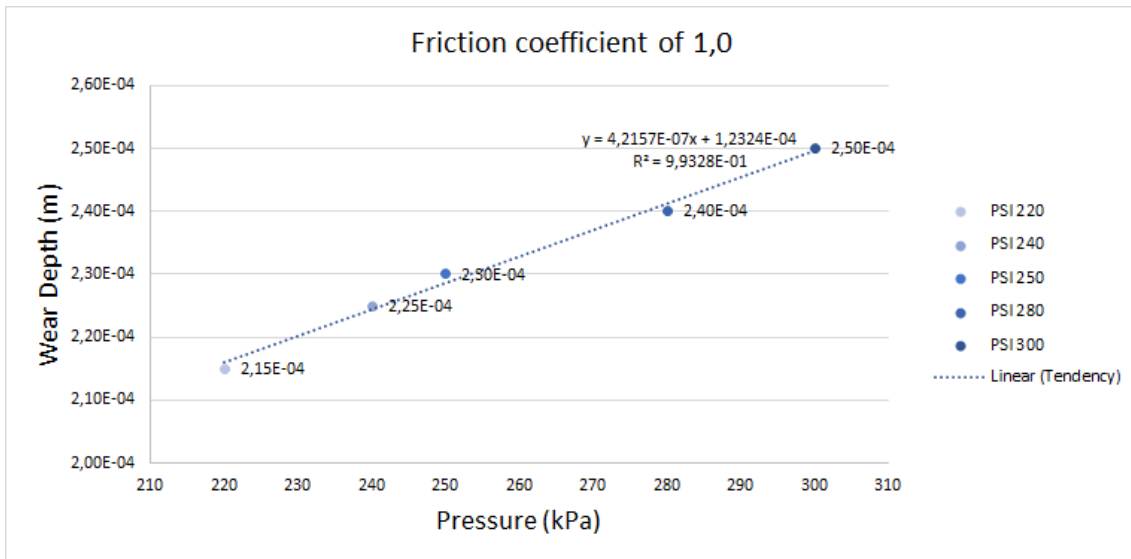
Figure 5.3: Wear depth in straight rolling with a friction coefficient of 1.0

Subsequent, the relationship between inflation pressure and wear rate maintains, with the addition that for higher friction coefficients, the wear depth tends to increase. Furthermore, the tendency line error is around 0,67%, making the results plausible.
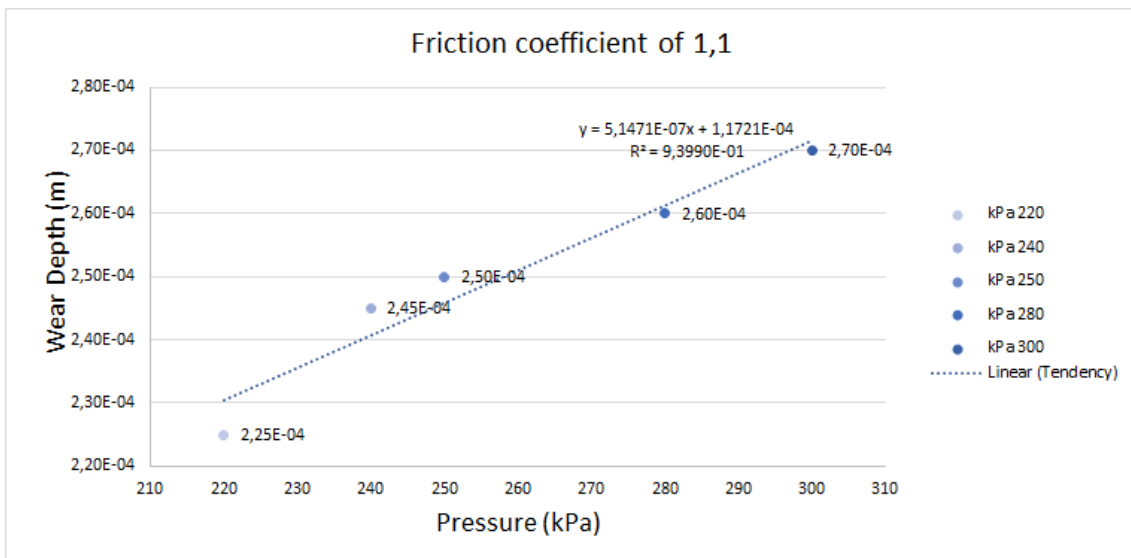
Figure 5.4: Wear depth in straight rolling with a friction coefficient of 1.1

For a friction coefficient of 1.1, the results follow the same trend as the results previously
obtained. The ablation tends to be higher with the the increase in the inflation pressure.
Although, the tendency line error, is quite larger, 6.01%, making the extrapolation of
results to another pressures, inaccurate.
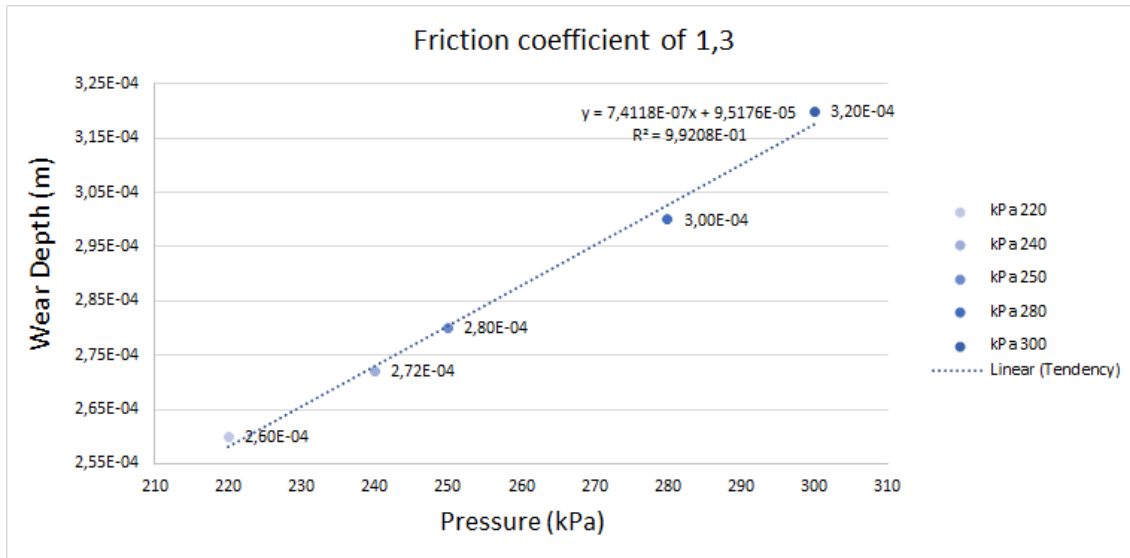
Figure 5.5: Wear depth in straight rolling with a friction coefficient of 1.3

Lastly, the maximum wear depth reaches its maximum values with a friction coefficient
of 1.3 (for the considered friction coefficients). The tendency line drawn with the five
different values for the wear depth/pressure, has an error of 0,79%, which is considerably
low, thus, the correlation with different pressures is plausible.

In conclusion, a tendency line was seen of the evolution of the displacement results,
obtained for each friction coefficient with corresponding pressure. From there, a primitive
mathematical equation was formulated with the corresponding fit error (the method of
least squares). The equations built with the tendency line presented credible results,
except for the friction coefficient of 1.1 (where the error was 6.017%). Finally, the
rolling distance is only 555,5 km, in order to save computation time, which makes this
results just a small sample when compared to the full extent of a tire life time millage.

Chapter 6

Conclusions

6.1   Achieved goals

Throughout the Dissertation the potential of the Abaqus software as an approach to wear prediction of a rolling tire was demonstrated. One of the biggest challenges was in tire modelling, since there is a lack of information regarding the tire components dimensions and material properties. Putting aside all of this setbacks, a model was developed in Abaqus software based on the geometrical and material properties described in the study proposed by Palanivelu *et al.* [2]. The FEM model was subjected to three different analysis. In the first one, a static analysis was conducted in order to study the change in the contact patch stress distribution when subjected to different inflation pressures. The results show that as the inflation pressure increases, the contact patch area tends to decrease, which in turn increases the normal force acting on the tire generated by the interaction tire-road.

Proceeding to the second analysis performed, the tire was subjected to a steady-state rolling analysis, besides the variation of the inflation pressure(220, 240, 250, 280 and 300 kPa), a variation in the friction coefficient on the interaction tire-road was added, varying between 0.8, 1.0, 1.1 and 1.3. The outcome from the performed analysis was that isolating the pressure with a varying friction coefficient, the contact pressure increases with an increase in the friction coefficient, although the contact patch geometry remains almost identical.

Lastly, the wear analysis provided good and consistent results. The wear depth obtained, after each run of a varying inflation pressure and friction coefficient, provided a clear demonstration of the direct relationship between friction coefficient and wear rate. As shown in the section 5.1, it was possible to formulate a primitive mathematical equation with a mimimum error to predict wear within each friction coefficient for different inflation pressures, except for a friction coefficient of 1.1 (where the fit error was 6.01%).

6.2   Future works

During the course of this Dissertation, many ideas have arisen from the setbacks and difficulties encountered. The following aspects are suggested to be included for future investigations, in order to take the full advantage of the FEM towards predicting tire wear in dry/wet conditions.

Firstly, the current model needs to be suitable for wet analysis. There are two possible ways to accomplish this goal, by introducing a previously obtained friction coefficient for the related pavement in a wet condition, or using an Smoothed Particle Hydrodynamics (SPH) for the water layer is introduced.

3D modelling of different tire sizes and treads can be used in order to fully comprehend the interaction between the road and the tire. Furthermore, an automated software framework can be established for importing the tire section geometrical properties. The automated framework can be achieved with Abaqus associative interfaces, like the Elysium plugin [24].

The effect of using different material models (like the Marlow hyperelasticity model) and different element types deserves a further investigation to find the most suitable discretization for the tire model. Moreover, to improve the accuracy of the results, anisotropic tire sections such as belts, ply and carcass needs to be further analyzed quantitatively. A more rigorous experimental material testing and modeling is suggested to enhance reliability of the model.

Finnaly, thermal elements can be added ito the FEM tire model in order to study the effects of the stress distribution and the behavior of the rubber under different contact temperatures.

Appendices

Appendix A

Static Footprint analysis - Abaqus input File

```
*HEADING
 SYMMETRIC RESULTS TRANSFER FOR TIRE MODEL
 3D HALF TIRE MODEL
 STEP 0: TRANSFER TIRE INFLATION RESULTS FROM
 STEP 1: BRING TRANSFERRED AXISYMMETRIC RESULTS
         TO EQUILIBRIUM
 STEP 2: FOOTPRINT ANALYSIS (DISPLACEMENT CONTROL)
 STEP 3: FOOTPRINT ANALYSIS (LOAD CONTROL)
 UNITS: KG, M
*RESTART,WRITE,FREQ=100
*NODE,NSET=ROAD
 9999,    0.0,    0.0, -0.340
*SYMMETRIC MODEL GENERATION,REVOLVE,ELEMENT=2000,NODE=2000
0.0, 0.0, 0.0,    0.0, 1.0, 0.0
0.0, 0.0, 1.0
120., 6,,g
 40., 8,,g
 40.,20,,g
 40., 8,,g
120., 6,,g
*SYMMETRIC RESULTS TRANSFER, STEP=1,INC=4
*SURFACE,TYPE=CYLINDER,NAME=SROAD
 0., 0.,-0.340,    0.340, 0.,-0.340
 0., 0.340,-0.340
 START, -0.4, 0.
 LINE,    0.4, 0.
*RIGID BODY,REF NODE=ROAD,ANALYTICAL SURFACE=SROAD
*CONTACT PAIR,INTERACTION=SRIGID
 OUTSIDE, SROAD
*SURFACE INTERACTION,NAME=SRIGID
```

```
∗FRICTION
 0.0
∗FILE FORMAT,ZERO INCREMENT
∗∗∗∗∗∗∗∗∗∗∗∗∗∗∗∗∗∗∗∗∗∗∗∗∗∗∗∗∗∗∗∗∗∗∗∗∗∗∗∗∗∗∗∗
∗STEP,INC=100,NLGEOM=YES
 1:  BRING TRANSFERRED RESULTS TO EQUILIBRIUM
∗STATIC, LONG TERM
 1.0, 1.0
∗BOUNDARY,OP=NEW
 RIM,  1, 6
 ROAD, 1, 6
∗DSLOAD,OP=NEW
 INSIDE, P, 250.E3
∗NODE PRINT,NSET=ROAD,FREQ=0
 U,
 RF,
∗EL PRINT,FREQ=0
∗OUTPUT,FIELD,FREQ=1
∗ELEMENT OUTPUT
 S,LE
∗NODE OUTPUT
 U
∗CONTACT OUTPUT,VAR=PRESELECT
∗OUTPUT,HISTORY,VAR=PRESELECT,FREQ=1
∗NODE OUTPUT, NSET=ROAD
 U,RF,CF
∗END STE
∗∗∗∗∗∗∗∗∗∗∗∗∗∗∗∗∗∗∗∗∗∗∗∗∗∗∗∗∗∗∗∗∗∗∗∗∗∗∗∗
∗STEP,INC=100,NLGEOM=YES
 2:  FOOTPRINT (Displacement controlled)
∗STATIC, LONG TERM
 1.0, 1.0
∗BOUNDARY,OP=NEW
 RIM,  1, 6
 ROAD, 1, 2
 ROAD, 4, 6
 ROAD, 3, , 0.03
∗END STEP
∗∗∗∗∗∗∗∗∗∗∗∗∗∗∗∗∗∗∗∗∗∗∗∗∗∗∗∗∗∗∗∗∗∗∗∗∗∗∗∗
∗STEP,INC=100,NLGEOM=YES
 3:  FOOTPRINT (Load controlled)
 ∗STATIC, LONG TERM
 1.0, 1.0
∗BOUNDARY,OP=NEW
 RIM,  1, 6
 ROAD, 1, 2
 ROAD, 4, 6
```

```
*CLOAD, OP=NEW
 ROAD, 3, 6000.
*END STEP
```

Intentionally blank page.

Appendix B

Steady-state rolling analisys - Abaqus input File

```
*HEADING
 STEADY-STATE ROLLING ANALYSIS OF A TIRE:
 STEP 1: FULL BRAKING ANALYSIS
 STEP 2: 2 DEGREE SLIP
 UNITS: KG, M
*RESTART,READ,STEP=3,WRITE,FREQ=999
*constraint controls, print=yes
*****************************************
*STEP,INC=300,NLGEOM=YES,UNSYMM=YES
 4:  STRAIGHT LINE ROLLING (Full braking)
*STEADY STATE TRANSPORT, INERTIA=NO
 0.1, 1.0
*CHANGE FRICTION,INTERACTION=SRIGID
*FRICTION,SLIP=0.02
 0.8
*TRANSPORT VELOCITY
 NTIRE, 27.34
*MOTION,TYPE=VELOCITY,TRANSLATION
 NTIRE, 1, , 11.11
*NODE PRINT,FREQ=0
*EL PRINT,FREQ=0
*OUTPUT,FIELD,OP=NEW,FREQ=10000
*ELEMENT OUTPUT
S,LE
*ELEMENT OUTPUT,REBAR
 S,LE
*Node Output
 U,V,COORD
*CONTACT OUTPUT
 CSTRESS,CDISP,CSTRESSERI
*OUTPUT,HISTORY,VAR=PRESELECT,FREQ=1
```

∗NODE OUTPUT, NSET=RIM
 U, RF
∗NODE OUTPUT, NSET=ROAD
 U, RF
∗END STEP

Appendix C

Abaqus wear subroutine

```
∗HEADING
∗restart ,read ,step=4
∗STEP, INC=300,NLGEOM=YES,UNSYMM=YES
  2:    ABLATION
∗STEADY STATE TRANSPORT,INERTIA=YES
  5E3 , 5E4 ,  , 5E3
∗RESTART,WRITE,FREQ=1
∗print ,contact=yes ,adapt=yes
∗adaptive mesh,elset=TREAD,FREQ=1,MESH=4
∗adaptive mesh constraint ,type=velocity ,user
NADAPT, 1 , ,5.555555E−14
∗adaptive mesh constraint ,constraint=lagrangian
NADAPT_LAGR,
∗END STEP
```

Intentionally blank page.

Appendix D

Abaqus wear subroutine

```
C        USER INPUT FOR ADAPTIVE MESH CONSTRAINT
C
         SUBROUTINE UMESHMOTION(UREF,ULOCAL,NODE,NNDOF,
     $        LNODETYPE,ALOCAL,NDIM,TIME,DTIME,PNEWDT,
     $        KSTEP,KINC,KMESHSWEEP,JMATYP,JGVBLOCK,LSMOOTH)
C
         include 'ABA_PARAM.INC'
C
C        USER DEFINED DIMENSION STATEMENTS
C
         CHARACTER*80 PARTNAME
C        The dimensions of the variables ARRAY
C        must be set equal to or greater than 15
         DIMENSION ARRAY(1000),JPOS(15)
         DIMENSION ULOCAL(*)
         DIMENSION UGLOBAL(NDIM)
         DIMENSION JGVBLOCK(*),JMATYP(*)
         DIMENSION ALOCAL(NDIM,*)
         DIMENSION WVLOCAL(3),WVGLOBAL(3)
         PARAMETER (NELEMMAX=100)
         PARAMETER (CHARLENGTH = 1.D-1,ELINC = 0.05D0)
         PARAMETER (ASMALL = 1.D-10)
         DIMENSION JELEMLIST(NELEMMAX),JELEMTYPE(NELEMMAX)
C
C        Wear topology common block and parameters
C
C        nstreamlines = number of points at the reference section
C        nGenElem     = number of general sectors in the model
C        nCylElem     = number of cylindrical sectors in the model
C                       (Cylindrical elements are not supported currently)
C        nRevOffset   = node offset specified under SMG,revolve
C        nReflOffset  = node offset specified under SMG,reflect
C                       (Set it to zero if the model is not reflected)
```

```
C       jslnodes      = The first component of this arry is the node number
C                       at the reference section. The second component is the
C                       Node thatprovides the wear direction. If the wear has
C                       to be applied in the normal direction, set it to zero.
C       endisp1       = Array of cumulative ablation magnitude for streamlines
C                       from the previous increment
C       endisp0       = Array of Cumulative ablation magnitude for streamlines
C                       from the current increment
C       enstrlen1     = Array of streamline lenghts from the previous increment
C       enstrlen0     = Array of streamline lengths from the current increment
C
        parameter ( nstreamlines=33,nGenElem=48,nCylElem=0,nRevOffset=2000,
     $   nReflOffset=0)
        common /wear/
     $       jslnodes(2,nstreamlines),
     $       endisp0(nstreamlines),endisp1(nstreamlines),
     $       enstrlen0(nstreamlines),enstrlen1(nstreamlines),
     $       lvalidinc,lvalidsweep
        data lvalidinc /-1/
        data jslnodes/
     $302, 0,
     $303 ,0,
     $304, 0,
     $305, 0,
     $306, 0,
     $55 ,46 ,
     $62 ,40 ,
     $366, 0,
     $367, 0,
     $368, 0,
     $369, 0,
     $63 ,36 ,
     $58 ,33 ,
     $359, 0,
     $360, 0,
     $361, 0,
     $59 , 0,
     $130, 0,
     $129, 0,
     $128, 0,
     $127, 0,
     $126, 0,
     $18 ,5 ,
     $61 ,8 ,
     $365, 0,
     $364, 0,
     $363, 0,
```

```
      $362 ,  0 ,
      $60 ,12 ,
      $64 ,1 ,
      $372 ,0 ,
      $371 ,0 ,
      $370 ,0 /
C
       NELEMS = NELEMMAX
       ldebug = 0
       jtyp = 0
       CALL GETNODETOELEMCONN(NODE,NELEMS,JELEMLIST,JELEMTYPE,
      $       JRCD,JGVBLOCK)
       luseendisp = 1
C       if (ldebug.ne.0) then
C         write (7,*) 'UMESHMOTION'
C         write (7,*) 'JELEMLIST␣'
C         do k1 = 1,NELEMS
C           write (7,*) JELEMLIST(k1)
C         end do
C         write (7,*) 'kstep␣',kstep
C         write (7,*) 'kinc␣',kinc
C         write (7,*) 'kmeshsweep␣',kmeshsweep
C         write (7,*) 'nstreamlines␣',nstreamlines
C         write (7,*) 'uref␣',uref
C
C        end if

       IF (KINC.EQ.1.AND.kmeshsweep.eq.0.and.lvalidinc.eq.−1) then
C         first time in this routine altogether
         lvalidinc = 2
         lvalidsweep = 1
         luseendisp = 0
       else if (kinc .eq. lvalidinc) then
C         first time in this routine this new increment
C         Move back copy of energy to front copy
         do k1 = 1,nstreamlines
           endisp1(k1) = endisp0(k1)
           endisp0(k1) = 0.0d0
           enstrlen1(k1)= enstrlen0(k1)
           enstrlen0(k1)= 0.0d0
         end do
         lvalidinc = kinc + 1
         lvalidsweep = 1
       end if
       if (kmeshsweep.eq.lvalidsweep) then
C         first time in this routine this mesh sweep
C         reset back copy of energy dissipation and streamline length
```

```fortran
        do k1 = 1,nstreamlines
          endisp0(k1) = 0.0d0
          enstrlen0(k1) = 0.0d0
          enstrlen1(k1)= enstrlen0(k1)
          enstrlen0(k1)= 0.0d0
        end do
        lvalidsweep = kmeshsweep + 1
      end if
      if (ldebug.ne.0) then
        write (7,*) 'lvalidinc ',lvalidinc
        write (7,*) 'lvalidsweep ',lvalidsweep
      end if

      LOCNUM = 0
      JRCD = 0
      PARTNAME = ' '
      PEEQ = 0.0D0
      CALL GETPARTINFO(NODE,0 ,PARTNAME,LOCNUM,JRCD)
      lstreamline = 0
      lposition = 0
      nslnodes=nGenElem+2*nCylElem
C     Which streamline is locnum on?
      do ksl = 1,nstreamlines
C     locnum > nReflOffset, node lies on the reflected half
          if ((locnum-nReflOffset).gt.0) then
C     process only jslnodes that are higher than nReflOffset
            if ((jslnodes(1,ksl)-nReflOffset).gt.0) then
          if (MOD((locnum-jslnodes(1,ksl)),nRevOffset).eq.0) then
            lstreamline=ksl
                lposition=1+(locnum-jslnodes(1,ksl))/nRevOffset
              end if
            end if
          else
C     locnum < nReflOffset, process only jslnodes less than nReflOffset
            if ((jslnodes(1,ksl)-nReflOffset).lt.0) then
              if (MOD((locnum-jslnodes(1,ksl)),nRevOffset).eq.0) then
                lstreamline=ksl
                lposition=1+(locnum-jslnodes(1,ksl))/nRevOffset
              end if
            end if
          end if
        end do
      if (ldebug.ne.0) then
        write (7,*) locnum, node, ' is on streamline ',lstreamline
        write (7,*) locnum, node, ' is at position   ',lposition
      end if
      if (lstreamline.eq.0) return
```

```fortran
         CALL GETVRMAVGATNODE(LOCNUM,JTYP,'CSTRESS ',ARRAY,JRCD,
     $        JELEMLIST,NELEMS,JMATYP,JGVBLOCK)
         CPRESS = ARRAY(1)
         CSHEAR = SQRT(ARRAY(2)**2+ARRAY(3)**2)
C        IF (CSHEAR.LT.ASMALL) GOTO 500
         CALL GETVRMAVGATNODE(LOCNUM,JTYP,'CDISP ',ARRAY,JRCD,
     $        JELEMLIST,NELEMS,JMATYP,JGVBLOCK)
         CSLIP = SQRT(ARRAY(2)**2+ARRAY(3)**2)
C        IF (CSLIP.LT.ASMALL) GOTO 500
C     Length of the streamline segment is 0.5*(distance_to_previous_node+distan
C
C        coordinates of locnum
         LTRN=0
         CALL GETVRN(LOCNUM,'COORD',ARRAY,JRCD,JGVBLOCK,LTRN)
         current_x=ARRAY(1)
         current_y=ARRAY(2)
         current_z=ARRAY(3)
C
C        coordinates of the previous point
         LPREV=0
         if (lposition.eq.1) then
            LPREV=LOCNUM+(nslnodes-1)*nRevOffset
         else
            LPREV=LOCNUM-nRevOffset
         end if
         CALL GETVRN(LPREV,'COORD',ARRAY,JRCD,JGVBLOCK,LTRN)
         prev_x=ARRAY(1)
         prev_y=ARRAY(2)
         prev_z=ARRAY(3)
C
C        coordinates of the next point...
         LNEXT=0
         if (lposition.eq.nslnodes) then
            LNEXT=LOCNUM-(nslnodes-1)*nRevOffset
         else
            LNEXT=LOCNUM+nRevOffset
         end if
         CALL GETVRN(LNEXT,'COORD',ARRAY,JRCD,JGVBLOCK,LTRN)
         cnext_x=ARRAY(1)
         cnext_y=ARRAY(2)
         cnext_z=ARRAY(3)
C
C        distances
         dist_prev= SQRT ((prev_x-current_x)**2+(prev_y-current_y)**2
     $        +(prev_z-current_z)**2)
         dist_next=SQRT((cnext_x-current_x)**2+(cnext_y-current_y)**2+
```

```
      $          ( cnext_z−current_z )∗∗2 )
         SL_LENGTH=0.5∗( dist_prev+dist_next )
c
c       This must also include the length of the streamline segment
         if ( ldebug . ne . 0 ) then
           write  ( 7 ,∗ )  'Adding␣' ,(SL_LENGTH) ,
      $        '␣to␣streamline␣' , lstreamline
           write  ( 7 ,∗ )  'Adding␣' ,(CSLIP ∗ CSHEAR ∗
      $          SL_LENGTH) , '␣to␣streamline␣' , lstreamline
         end if
C
         ENSTRLEN0( lstreamline )  =  ENSTRLEN0( lstreamline ) +
      $        (SL_LENGTH)
C
         ENDISP0( lstreamline )  =  ENDISP0( lstreamline ) +
      $        (CSLIP ∗ CSHEAR ∗ SL_LENGTH)
C
  500    if ( luseendisp . ne . 0 ) then
            ldebug2 = 0
            if ( ldebug . ne . 0 ) ldebug2 = 1
            if ( ldebug . ne . 0 ) then
              write  ( 7 ,∗ )  'Ablating␣node␣' ,
      $            locnum , ENDISP1( lstreamline ) ∗ UREF
              write  ( 7 ,∗ )  'alocal'
              write  ( 7 ,100 )  alocal ( 1 ,1 ) , alocal ( 1 ,2 ) , alocal ( 1 ,3 )
              write  ( 7 ,100 )  alocal ( 2 ,1 ) , alocal ( 2 ,2 ) , alocal ( 2 ,3 )
              write  ( 7 ,100 )  alocal ( 3 ,1 ) , alocal ( 3 ,2 ) , alocal ( 3 ,3 )
  100         format  ( 1x ,3 ( 1 pg15 .2 ) )
            end if
C
            if (ABS( enstrlen1 ( lstreamline ) ) . lt .ASMALL) then
               SURFV=0.0d0
            else
               SURFV = ENDISP1( lstreamline ) ∗ UREF / enstrlen1 ( lstreamline )
            end if
C
C   Wear Direction :
C   Ablate the node along ULOCAL( 3 ) if there is no dependency .
C   Else , compute the wear direction in the global system , apply the wear
C   and transform it back to the local system
C
            if ( jslnodes ( 2 , lstreamline ) . eq . 0 ) then
               ULOCAL(NDIM)=ULOCAL(NDIM)−SURFV
            else
C   Compute the node number of the wear master
               Master=(lposition −1)∗nRevOffset+jslnodes ( 2 , lstreamline )
               LTRN=0
```

```fortran
            CALL GETVRN(MASTER, 'COORD' ,ARRAY,JRCD,JGVBLOCK,LTRN)
            cmaster_x=ARRAY(1)
            cmaster_y=ARRAY(2)
            cmaster_z=ARRAY(3)
            dist_master=SQRT((cmaster_x-current_x)**2+
     $           (cmaster_y-current_y)**2+(cmaster_z-current_z)**2)
C   Wear in Global directions
            WVGLOBAL(1)=SURFV*(cmaster_x-current_x)/dist_master
            WVGLOBAL(2)=SURFV*(cmaster_y-current_y)/dist_master
            WVGLOBAL(3)=SURFV*(cmaster_z-current_z)/dist_master
C   Transformation to the local directions
            do k2=1,NDIM
                WVLOCAL(k2)=0
                do k3=1,NDIM
                    WVLOCAL(k2)=WVLOCAL(k2)+WVGLOBAL(k3)*ALOCAL(k3,k2)
                end do
            end do
            do k2 = 1,ndim
                ULOCAL(k2) = ULOCAL(k2) + WVLOCAL(k2)
            end do
         end if
C
C       SHARE OF ELEMENT CONSUMED IN NEXT INCREMENT
        PELEM = DTIME * SURFV / CHARLENGTH
        PNEWDT0 = PNEWDT
        PNEWDT1 = 0.0D0
        IF (PELEM.GT.ELINC.AND.SURFV.GT.0.0D0) THEN
          PNEWDT1 = CHARLENGTH * ELINC / SURFV
          IF (PNEWDT1.LT.PNEWDT0) THEN
            WRITE (7,*) 'CHANGING TIME INCREMENT FROM ',PNEWDT0
            PNEWDT = PNEWDT1
            WRITE (7,*) 'TO ',PNEWDT
            WRITE (7,*) 'BASED ON NODE ',LOCNUM
          END IF
        END IF
       end if
C
      RETURN
      END
```

Intentionally blank page.

Bibliography

[1] A. N. Gent and J. D. Walter. Mechanical properties of rubber. In *The Pneumatic Tire*. National Highway Traffic Safety Administration U.S. Department of Transportation, 2005. URL `http://www.safetyresearch.net/Library/ACS_Pneu_Tire.pdf`.

[2] Sakthivel Palanivelu, K. V. Narasimha Rao, and Krishna Kumar Ramarathnam. Determination of rolling tyre modal parameters using Finite Element techniques and Operational Modal Analysis. *Mechanical Systems and Signal Processing*, 64-65:385–402, 2015. ISSN 10961216. doi: 10.1016/j.ymssp.2015.04.006.

[3] Chang Jin, Chenyuan Hou, and Xiaoxiong Jin. FE simulation of tire wear with complicated tread pattern. 15:5015–5019, 2011. ISSN 18777058. doi: 10.1016/j.proeng.2011.08.932.

[4] Hussain Kanchwala. Invention of Wheel: Why and When Was the Wheel Invented. URL `https://www.scienceabc.com/innovation/how-was-the-wheel-invented.html`. Last visited 2019-03-20.

[5] History - Continental AG. URL `https://www.continental-corporation.com/en/company/history`. Last visited 2019-03-20.

[6] Tyre history. URL `https://www.longstonetyres.co.uk/vintage-tyres.html`. Last visited 2019-03-20.

[7] The Pneumatic Tire. 2006. URL `https://www.fueleconomy.gov/feg/pdfs/PneumaticTire_HS-810-561.pdf`.

[8] Alberto Doria, Luca Taraborrelli, Tarek Jomaa, Tom Peijs, Mario Potter, Sunjoo Advani, and Larry Crichlow. Identification of the Mechanical Properties of Tires for Wheelchair Simulation. *The Open Mechanical Engineering Journal*, 10(1):183–200, 2017. ISSN 1874-155X. doi: 10.2174/1874155x01610010183.

[9] Paul Haney. Inside racing technology, 2004. URL `http://insideracingtechnology.com/tirebkexerpt1.html`. Last visited 2019-05-12.

[10] Valentin L. Popov. *Contact Mechanics and Friction*. Springer Berlin Heidelberg, Berlin, Heidelberg, 2010. doi: 10.1007/978-3-642-10803-7_10.

[11] Ing R T Uil, I J M Besselink, and J A W Van Dommelen. *Tyre models for steady-state vehicle handling analysis*. PhD thesis, Eindhoven University of Technology / TNO Automotive, 2007.

[12] Hans B. Pacejka and Egbert Bakker. The Magic Formula tyre model. *Vehicle System Dynamics*, 21(1):1–18, 1992. ISSN 0042-3114. doi: 10.1080/00423119208969994. URL `http://www.tandfonline.com/doi/abs/10.1080/00423119208969994`.

[13] Archard Wear Equation. URL `https://www.tribonet.org/wiki/archard-wear-equation/`. Last visited 2019-04-14.

[14] Adaptive Meshing and Distortion Control Lecture 6, 2005. URL `https://imechanica.org/files/l6-adaptive-mesh.pdf`.

[15] How A Tire Is Made, Michelin US. URL `https://www.michelinman.com/US/en/help/how-is-a-tire-made.html`. Last visited 2019-04-02.

[16] What's In a Tire, U.S. Tire Manufacturers Association. URL `https://www.ustires.org/whats-tire-0`. Last visited 2019-04-04.

[17] Hyperelastic materials — SimScale Documentation. URL `https://www.simscale.com/docs/content/simulation/model/materials/hyperelasticMaterial.html`. Last visited 2019-04-01.

[18] Abaqus. Abaqus 6.13 example problems manual. URL `https://www.sharcnet.ca/Software/Abaqus610/Documentation/docs/v6.10/books/exa/default.html`. Last visited 2019-05-16.

[19] Bbanerje. Stress-strain relations for hyperelastic materials under uniaxial stretch, 2010. URL `https://commons.wikimedia.org/wiki/File:Hyperelastic.svg`. Last visited 2019-04-05.

[20] Abbas Samani, David Holdsworth, Kenneth Mcisaac, and Shaun Salisbury. *Soft Tissue Hyperelastic Parameter Reconstruction Technique for Breast Cancer Assessment*. PhD thesis, The University of Western Ontario, 2008. URL `http://citeseerx.ist.psu.edu/viewdoc/download?doi=10.1.1.473.733&rep=rep1&type=pdf`.

[21] Beomkeun Kim, Seong Beom Lee, Jayone Lee, Sehyun Cho, Hyungmin Park, Sanghoon Yeom, and Sung Han Park. A comparison among neo-hookean model, mooney-rivlin model, and ogden model for chloroprene rubber. *International Journal of Precision Engineering and Manufacturing*, 13(5):759–764, 2012. doi: 10.1007/s12541-012-0099-y.

[22] Rafael Tobajas, Elena Ibartz, and Luis Gracia. A comparative study of hyperelastic constitutive models to characterize the behavior of a polymer used in automotive engines. page A002, 05 2016. doi: 10.3390/ecm-2-A002.

[23] Kenneth H. Huebner and Kenneth H. Huebner. *The finite element method for engineers*. J. Wiley, 2001. ISBN 9780471370789.

[24] Elysium, multi-CAD data exchange solution. URL `https://www.elysium-global.com/en/`. Last visited 2019-06-16.